NASA Contractor Report 159184

THEORETICAL STUDY OF AERODYNAMIC CHARACTERISTICS
OF WINGS HAVING VORTEX FLOW

C. Subba Reddy

OLD DOMINION UNIVERSITY RESEARCH FOUNDATION
Norfolk, Virginia 23508

NASA Contract NAS1-14193-Task 48
November 1979

National Aeronautics and
Space Administration

Langley Research Center
Hampton, Virginia 23665

SUMMARY

The aerodynamic characteristics of slender wings having separation-induced vortex flows are investigated by employing three different computer codes—free vortex sheet, quasi-vortex lattice, and suction analogy methods. Their capabilities and limitations are examined, and they are modified and improved to a limited extent.

Flat wings of different configurations: arrow, delta and diamond shapes, as well as cambered delta wings, are studied. The effect of notch ratio on the load distributions and the longitudinal characteristics of a family of arrow and diamond wings is explored. The sectional lift coefficients and the accumulated span loadings are determined for an arrow wing and are seen to be unusual in comparison with the attached flow results. A pitch-up tendency is exhibited by arrow as well as diamond wings. The theoretically predicted results are compared with the existing experimental values and found to agree favorably up to moderate angles of attack; however, the codes tend to overpredict the pitching moment.

INTRODUCTION

Many modern aircraft designed for supersonic speeds employ highly sweptback and low aspect ratio wings with sharp or thin edges. Flow separation occurs near the leading and tip edges of such wings over a wide angle of attack range. The separation produces vortex sheets that roll up into strong vortices above the wing surface. These vortices produce regions of low pressure over the upper surface of the wing, thereby generating additional lift which is responsible for the well-known nonlinear aerodynamic characteristics.

In the design of high-speed aircraft, a detailed knowledge of the effect of separation-induced vortex flow on the wing flow field is needed to predict the performance under various operating

conditions. As the attached flow theories are inadequate for these conditions, the designer must rely presently on extensive and costly wind-tunnel tests for the required data. Therefore, attempts have been made over the years to develop analytical methods to predict the aerodynamic characteristics of such aircraft. They have met with varying degrees of success. A brief summary of some of the more successful methods is given in the next section. However, before any method can be useful, it must be tested against a standard set of data to determine its capabilities and limitations. In this paper, such an investigation is undertaken for the free vortex sheet, quasi-vortex lattice, and suction analogy methods.

Mostly wings for which experimental data is available are selected for this study so that a direct comparison can be made. They include flat wings of different configurations: delta, arrow and diamond, as well as cambered deltas. The effect of notch ratio on the longitudinal characteristics of a family of arrow and diamond wings is also investigated. The sectional lift coefficient and accumulated span loading for an arrow wing are calculated to determine how the sectional lift influences the overall characteristics and how span loading for separated flow differs from that from attached flow.

SYMBOLS

a	notch height
a/ℓ	notch ratio
A	aspect ratio
b	wing span
$b(x)$	local wing span
c	local wing chord
$\bar{c}$	mean aerodynamic chord
c_ℓ	sectional lift coefficient

c_{ℓ_a}	accumulated sectional lift coefficient
c_r	wing root chord
C_D	drag coefficient
C_L	lift coefficient
C_m	pitching moment coefficient
C_p	pressure coefficient
FVS	free vortex sheet
ISIDE	parameter that determines the matching of network sides
ℓ	distance between apex and tip along x-axis
LE	leading edge
M	Mach number
QVL	quasi-vortex lattice
Re	Reynolds number
S	wing area
SA	suction analogy
TE	trailing edge
x,y,z	body axis coordinates
α	angle of attack
ΔC_D	drag due-to-lift coefficient
ΔC_p	difference between upper and lower surface pressure coefficients
Λ	leading-edge sweep angle

THEORETICAL METHODS

Presented in this section are the methods employed in the present study together with some of their limitations and the improvements made in the numerical codes.

The Free Vortex Sheet (FVS) Method

The FVS Method (refs. 1 and 2), developed by Boeing Airplane Company under a contract with NASA/Langley Research Center (LaRC), is based on a three-dimensional inviscid flow model. This is an advanced panel method using distributed doublet singularities located on the mean surface of the wing and the free vortex sheet. It is capable of computing forces, moments, and surface pressures.

It should be mentioned here, however, that the FVS method is in the process of being modified to improve its capabilities. In the present investigation the available six-parameter version of the method is used.

While modeling a wing by the FVS method, 30 panels per half wing are generally used; in a limited number of cases, 48 or 60 panels are employed. A general rule regarding solution convergence is as follows: solutions not converging after five iterations are continued for another five iterations, provided the rate of convergence is fast enough; otherwise, the solution is discontinued and treated as nonconvergent. The solution is considered to be converged if the sum of the squares of the residuals is of the order of 10^{-3} or less. These residuals are proportional to the nonzero values of the pressure coefficient jump across the shed vortex system and the nonzero values of the normal velocities on the wing panels.

The FVS method adequately predicts the aerodynamic characteristics of low aspect ratio wings at moderate angles of attack. However, it is incapable of successfully modeling wings with high aspect ratios, low leading edge sweep angles and/or streamwise tips, nor can it handle large cambered wings. For example, no converged solutions are obtained for a delta wing of aspect ratio 4 and a 45° cropped delta wing of aspect ratio 1.33 at angles of attack of 10.36° and 20.83° respectively. It does not work for A = 1.46 delta wing at an angle of attack of 5°, but works for A = 1 delta wing at the same angle. This suggests an

inherent limitation in the FVS method that is α and Λ dependent. This dependency may be of the form $\tan \alpha \tan \Lambda$. The limitation acts to establish a lower α bound for which solutions are calculable. It should be pointed out that this α increases for planar delta wings as the sweep angle decreases. The FVS method successfully handles Squire's wings 1 to 4 (ref. 3), but not wings 6 and 7, which have larger camber. It is able to give converged results for wing 5 at a few angles of attack only after experimenting with different values of the perturbation parameter, APC (figure 17 of ref. 1).

It appears that the density and type of wing paneling have some influence on the solution given by the method. Table 1 shows the effect of such paneling. In case 1, 30 wing panels are considered with 7 rows and 6 columns, and this number is doubled in two ways as indicated in cases 2 and 3. While converged results close to those for case 1 are obtained in case 2, no such convergence is seen in case 3. Increasing the number of columns also increases the number of panels in the free and fed sheets and does not help to obtain converged solutions.

The results obtained by applying the FVS method with and without the "design" wake are compared with the experimental values of Wentz (ref. 4) in table 2. The use of the design wake does not provide any appreciable improvement in the accuracy of the theoretical lift and drag coefficients, but the pitching moment coefficient obtained by using the design wake is in better agreement with the data. In addition, the pressure distributions obtained with and without the design wake are significantly different near the wing trailing edge, as expected, but not near the apex, as illustrated in figure 1.

ISIDE (ref. 5) is one of the input parameters to the program. It should be set to zero or some other appropriate value. It appears that the parameter has little effect on the results. For example, $C_L = 0.885$ for an 80°/65° flat, double delta wing at $\alpha = 15°$ with ISIDE = 0, and $C_L = 0.921$ with ISIDE = appropriate

value; convergence is better in the latter case although neither case produces results which satisfy the convergence criterion.

Kuhlman (ref. 6) has developed a simplified input format for use in this program to generate cambered surfaces for general 3-D wings, Barsby's (ref. 7) and Wentz's (refs. 8 and 9) wings. In this paper the capability to model Squire's wings (ref. 3) has been added (see Appendix).

The Quasi-Vortex Lattice (QVL) Method

The QVL Method (refs. 10 and 11) predicts the aerodynamic characteristic pressures as well as integrated results of low-aspect ratio wings with partial leading edge separation in a steady inviscid flow. Here the wing is represented by a bound vortex sheet, across which there exists a pressure differential, and the separated flow along the leading edge by a force-free vortex sheet. The trailing wake is also force free. The method uses an interative procedure.

The number of spanwise lines, NSW, which is one of the important input parameters to this program, is dependent upon the aspect ratio. It can be taken from figure 14 in reference 11 for delta wings with aspect ratios up to 2. But if arrow and diamond wings are to be modeled successfully, curves similar to the one just mentioned must be constructed for each type of wing by a trial-and-error procedure. It is observed that NSW is greater for an arrow wing and less for a diamond wing than that for a delta wing of same aspect ratio.

Earlier this program could handle only flat delta wings; however the code has been improved to model arrow and diamond wings, including the camber effects as well. Most of the modifications are incorporated in the program itself; the rest are in the deck labeled "*IDENT CSR."

The Suction-Analogy *(SA) Method

The SA Method (refs. 12-15), developed at NASA/LaRC, estimates the overall forces and moments of complex planforms. However, it does not provide detailed surface pressure distributions. The planforms include wings with variable sweep, changes in dihedral angle across the span, twist and/or camber and also wings in conjunction with a tail or a canard. The method is based on a steady inviscid flow and represents the lifting surfaces with a vortex lattice (refs. 14 and 15).

The improvement made to this method is to develop a small subroutine which calculates the local angles of attack given the equation of the wing camber. This eliminates the need to supply such angles at each control point as input data to this program.

RESULTS AND DISCUSSION

In this section, the results obtained by employing the three numerical codes are compared with the existing data and also with the theoretical (published) results of vortex lattice (VL) method (refs. 16 and 17) wherever possible.

A summary of the various wing configurations investigated using different computer codes is presented in tables 3 to 5. The range of angle of attack and aspect ratio over which the codes are employed and whether or not the solutions given by the FVS and QVL methods are converged are also indicated in the tables.

Flat Wings

The lift and pitching moment coefficients for an A = 1 flat delta wing are shown in figure 2. The theoretical results obtained by using the VL (ref. 16), FVS, QVL and SA methods are compared with the experimental values of Peckham (ref. 18) and

---

* The term "suction analogy" usually refers to the method that calculates only vortex lift. However, for convenience, it is used here to identify the method which employs suction analogy concept to predict vortex lift in combination with potential flow lift. The potential flow method used herein is that of reference 15.

Tosti (ref. 19) over an angle of attack range of 0° to 30°. There is a fairly good agreement for lift coefficient between the data and all of the theoretical results over most of the investigated range of angle of attack. However, at higher angles of attack, the FVS method underpredicts, the SA method overpredicts, and the QVL method is in close agreement with the data for C_L. The pitching moment coefficient by the FVS and QVL methods agrees more favorably with the data than that by SA method, especially at higher angles of attack.

Figures 3 and 4 show the spanwise pressure distributions for a flat delta wing. Figure 3 compares the theoretical pressure coefficient values obtained by the FVS, QVL and VL (ref. 17) methods at a 15° angle of attack at two chordwise stations. The results given by the FVS and VL methods are in good agreement at $x/c_r = 0.7$ and over most of the span at $x/c_r = 0.82$. The QVL method does not give a pronounced peak in ΔC_p as the others do. In figure 4 pressure distributions by the FVS method are compared with the experimental values of Nangia (ref. 20) at an angle of attack of 22.5° at 2 chordwise stations. As can be seen from the figure, there is no good agreement between the theory and the data, especially around $2y/b(x) = 0.6$.

The longitudinal aerodynamic characteristics and spanwise pressure distributions for a flat wing of aspect ratio 1.46 are shown in figures 5 and 6 respectively. The lift coefficient values predicted by the FVS, QVL, and SA methods compare fairly well with the data of Wentz (ref. 4) in the angle-of-attack range from 0° to 30°. But, the theoretical values of pitching moment deviate from the data, especially at higher angles of attack. The FVS method gives a pressure distribution which is in better agreement with the data of Marsden et al. (ref. 21) than that by the QVL and VL (ref. 17) methods. However, the peak values of ΔC_p given by the FVS method are greater than either the data or those given by the other methods, and this is indicative of the equivalent vortex core representation in the FVS method.

A comparison is made in figures 7 and 8 between Wentz's data (ref. 4) and the longitudinal aerodynamic characteristics predicted by the 3 codes for arrow and diamond wings over an angle-of-attack range of 0° to 40°. There is a good agreement between the theoretical and experimental C_L and ΔC_D at lower angles of attack in both the cases of arrow and diamond wings; but, at higher angles of attack, all three codes overpredict C_L, ΔC_D and C_m to various degrees for arrow wings. The FVS method agrees well with C_L and ΔC_D data even at higher angles of attack for diamond wings. The pitching moment values given by QVL method are in better agreement than those given by the other methods for both wings.

Figures 9 to 12 illustrate the longitudinal aerodynamic characteristics of a family of arrow and diamond wings and notch ratios varying from -0.273 to 0.455 over an angle-of-attack range of 0° to 40°. These wings are investigated by the FVS and SA methods only and not by the QVL method due to computational cost considerations. The C_L and C_m results obtained by both methods are plotted against notch ratio in figures 9 and 10 without comparison to any data as the data available is limited to wings with $a/\ell = -0.273$ and 0.455. Comparisons between data and theory for these wings are given in figures 7 and 8. Though the SA method predicts higher values, both the methods generally show the same trend: as the notch ratio increases, C_L and C_m decrease in general. However, at higher angles of attack, these values increase as the notch ratio increases from -0.273 to about 0. Figure 11 illustrates the pitching characteristics for wings with different notch ratios. The FVS method shows pitch-up for both the arrow and diamond wings whereas the other method does not. The lift characteristics obtained by the SA method with and without augmentation effect (ref. 12) are compared with those by the FVS method in figure 12. The FVS method predicts higher lift than the SA method, when no augmentation is considered, for diamond wings except at high angles of attack. However, when the augmentation effect is taken into account, the SA method gives higher values for almost all the wings.

The results presented in figures 13 to 28 are obtained by the FVS method for a family of arrow and diamond wings. The dashed lines on the planforms shown in the figures correspond to the locations where the pressures or the span loadings are illustrated. The pressure distributions on upper and lower surfaces of arrow wings (a/ℓ = -0.273 to 0.0) are shown in figures 13 to 16. These results are obtained at various chordwise locations at an angle of attack of 25°. As the pressures are not available at the same chordwise stations for each arrow wing, a direct comparison cannot be easily made.

The effect of notch ratio on the surface pressures for diamond wings (a/ℓ = 0.10 to 0.455) is shown in figures 17 to 19. As can be seen from the figures, the pressure coefficients at chordwise locations of x/ℓ = 0.167 and 0.5 are independent of the notch ratio. Only near the trailing edge is the pressure distribution slightly affected by the notch ratio. Figure 20 also depicts the pressures near the trailing edge for both the arrow and diamond wings and shows that ahead of the tip a diamond wing develops higher $-\Delta C_p$ than an arrow, as expected. A similar trend can also be seen on the right side of the figure for arrow wings as the notch ratio tends to 0.

The spanwise as well as surface pressure distributions are given in figures 21 and 22 for an arrow wing with notch ratio of -0.273 at an angle of attack of 35°. Using these two figures, figure 23 is constructed which illustrates the chordwise pressure distributions. (As the FVS method provides pressures only at constant x locations along the radial lines emanating from the wing apex, it becomes necessary to go through the above procedure to obtain the chordwise pressure distributions.) Diagrams similar to figures 21 to 23 are drawn at various angles of attack (but here only the latter are shown as the samples) to estimate the sectional lift coefficient and accumulated span loadings which are important in determining the root bending moment and in other design considerations.

Figure 24 depicts the variation of the sectional lift coefficient, c_ℓ, with angle of attack for an arrow wing at three different spanwise stations; c_ℓ is obtained from the equation

$$c_\ell = \frac{1}{c}\int_{LE}^{TE} -\Delta C_p \, dx$$

by integrating with a planimeter the area under the curves in figure 23 and the similar curves at other angles of attack. As can be noticed from the figure, the rate of increase of c_ℓ with respect to α increases inboard and decreases outboard at higher α. This may partially explain the pitch-up tendency of arrow planforms noticed in figure 11.

Figures 25 to 28 show the accumulated sectional lift distribution $c_{\ell_a} c$, for an arrow wing at different angles of attack; c_{ℓ_a} is calculated from the equation

$$c_{\ell_a} = \frac{1}{c}\int_{LE}^{x'} -\Delta C_p \, dx$$

where x' is distance along the plane of symmetry and varies between 0 and ℓ depending upon the chordwise locations at which c_{ℓ_a} is desired. This is also evaluated as described in the above paragraph. These span loadings are unusual in comparison with the attached flow results. The slopes of the curves near the leading edge are also important in that they do not tend to infinity as they do in attached flow.

Spanwise Cambered Wings

Nangia's Type

As it is more convenient and accurate to prepare the input data with the equation describing the wing camber than otherwise,

the following polynomial in x and y is developed and used in the investigation of Nangia's spanwise cambered delta wing (ref. 20):

$$z\ (x,y) = 2b(x)\ \left[0.05 + 0.0125\ \left|\frac{y}{b(x)}\right| - 0.1979\ \left|\frac{y}{b(x)}\right|^2 + 0.3698\ \left|\frac{y}{b(x)}\right|^3 - 0.3646\ \left|\frac{y}{b(x)}\right|^4 + 0.1302\ \left|\frac{y}{b(x)}\right|^5\right]$$

where $b(x) = 0.25x$.

Figure 29 compares the lift coefficient obtained by the FVS, QVL and SA methods with the experimental values of Nangia (ref. 20) for the wing. All the theoretical values are lower than the data, though FVS method shows a better agreement. The figure also shows theoretical pitching moments for the same wing; no corresponding data is available.

Squire's Wings

The camber surfaces of Squire's seven wings (ref. 3) are given by the equation

$$\frac{z}{cx} = -\beta\left(\frac{y}{cx}\right)^n$$

where x is measured along the plane of symmetry from the apex, y spanwise and z vertically upwards; β and n are constants for a given wing; and c is the tangent of the semi-angle of the apex of the planform. These constants are given in table 6.

The longitudinal aerodynamic characteristics of these seven spanwise cambered delta wings are presented in figures 30 to 36. Here the theoretical results, wherever available, are compared with Squire's experimental values. The data is available for an angle-of-attack range of 0° to 20°. The agreement between

the theories and the data is good. Only the SA method is employed to investigate all seven wings, and the results are obtained for them all. But the FVS method works only for wings 1 to 4 and partly for wing 5, and the QVL method is not used to model all the wings for lack of time.

CONCLUSIONS

All three numerical codes successfully predict the aerodynamic characteristics of low aspect ratio wings up to moderate angles of attack. However, they generally overpredict the pitching moment. The details are given below.

The six-parameter version of the free vortex sheet method seems to be incapable of handling wings with high aspect ratios, low leading edge sweep angles, and/or streamwise tips. It requires comparatively large computational time and input data. It does, however, predict better surface pressure distributions than the quasi-vortex lattice method.

The quasi-vortex lattice method can model low aspect ratio, arrow, delta, and diamond wings, but more study is required before it can conveniently be used for arrow and diamond wings. It needs the least amount of input data and provides only the net pressure acting on the wing, unlike the free vortex sheet method which gives upper and lower surface pressures.

The suction analogy method predicts results which are considerably greater than those given by the other methods at higher angles of attack. It takes the least amount of computational time and can handle even complex configurations which the other methods cannot, but does not give the detailed surface load distribution.

A series of wings with trailing edge notch is investigated, and the sectional lift coefficients and accumulated span loadings are determined for an arrow wing using the free vortex sheet method. The effect of increasing notch ratio is to decrease the

lift and pitching moment coefficients. The span loadings are unusual in comparison with the attached flow results. Another interesting aerodynamic feature is that a pitch-up tendency is exhibited for arrow as well as diamond wings.

No firm conclusions are drawn regarding the code capabilities at higher angles of attack because of insufficient data for the configurations tested in the range. Additional investigations are needed in this respect.

APPENDIX

THE FVS METHOD MODIFICATION

The program modifications are contained in the deck labeled "*IDENT DIM3D." The instructions for input data preparation are as follows, and they should be read in conjunction with those given in reference 6.

Put CNTRL = 5.0 to model a spanwise cambered delta wing (ref. 3) whose surface is described by the equation

$$z = -\beta\varepsilon x \left(\frac{y}{\varepsilon x}\right)^n$$

while β, ε and n are constants. One more card is then required to specify the constants as shown below (format 6F10.5):

Card	Columns	Variables
5	1-30	β,ε,n

REFERENCES

1. Brune, G.W.; Weber, J. A.; Johnson, F.T.; Lu, P.; and Rubbert, P. E.: A Three-Dimensional Solution of Flows over Wings with Leading-Edge Vortex Separation. Part I. Engineering Document, NASA CR-132709, 1975.

2. Weber, J. A.; Brune, G. W.; Johnson, F. T.; Lu, P.; and Rubbert, P. E.: A Three-Dimensional Solution of Flows over Wings with Leading-Edge Vortex Separation. AIAA Paper 75-866 (Hartford, Conn.), June 16-18, 1975.

3. Squire, L. C.: Camber Effects on the Nonlinear Lift of Slender Wings with Sharp Leading Edges. Aeronautical Research Council C.P. No. 924, Ministry of Technology (London), 1967.

4. Wentz, W. H. Jr.; and Kohlman, D. L.: Wing-Tunnel Investigation of Vortex Breakdown on Slender Sharp-Edged Wings. NASA CR-98737, 1968.

5. Johnson, F. T.; Lu, P.; and Rubbert, P. E.: An Improved Method for the Prediction of Completely Three-Dimensional Aerodynamic Load Distributions of Wings with Leading-Edge Vortex Separation. Program Usage Instructions prepared under NASA contract No. NAS1-13833.

6. Kuhlman, J. M.: Analytical Studies of Separated Vortex Flow on Highly Swept Wings. NASA CR 3022, Nov. 1978.

7. Barsby, J. E.: Flow Past Conically Cambered Slender Delta Wings with Leading-Edge Separation. ARC Reports and Memoranda No. 3748, 1972.

8. Wentz, W. H.: Effects of Leading-Edge Camber on Low Speed Characteristics of Slender Delta Wings. NASA CR-2002, 1972.

9. Wentz, W. H.: Effects of Leading-Edge Camber on Low Speed Characteristics of Slender Delta Wings—Techniques and Tabulated Data. NASA CR-112016, 1972.

10. Mehrotra, S. C.; and Lan, C. E.: A Computer Program for Calculating Aerodynamic Characteristics of Low-Aspect Ratio Wings with Partial Leading-Edge Separation. NASA CR-145362, 1978.

11. Mehrotra, S. C.; and Lan, E. E.: A Theoretical Investigation of the Aerodynamics of Low Aspect-Ratio Wings with Partial Leading-Edge Separation. NASA CR-145304, 1978.

12. Lamar, J. E.: Some Recent Applications of the Suction Analogy to Vortex-Lift Estimates. NASA SP-347, Part II, pp. 985-1011, 1975.

13. Polhamus, E. C.: A Concept of the Vortex Lift of Sharp-Edge Delta Wings Based on a Leading-Edge Suction Analogy. NASA TN D-3767, 1966.

14. Margason, R. F.; and Lamar, J. E.: Vortex-Lattice Fortran Program for Estimating Subsonic Aerodynamic Characteristics of Complex Planforms. NASA TN D-6142, 1971.

15. Lamar, J. E.; and Gloss, B. B: Subsonic Aerodynamic Characteristics of Interacting Lifting Surfaces with Separated Flow Around Sharp Edges Predicted by a Vortex-Lattice Method. NASA TN D-7921, 1975.

16. Kandil, O. A.; Mook, T. D.; and Nayfeh, A. H.: Nonlinear Prediction of the Aerodynamic Load of Lifting Surfaces. AIAA Paper 74-503, 1974.

17. Kandil, O. A.; Mook, T. D.; and Nayfeh, A. H.: New Convergence Critera for the Vortex Lattice Methods of the Leading Edge Separation. NASA SP-405, 1976.

18. Peckham, D. H.: Low-Speed Wind-Tunnel Tests on a Series of Uncambered Slender Pointed Wings with Sharp Edges. ARC R & M 3186, 1961.

19. Tosti, L. P.: Low-Speed Static Stability and Damping-in-Roll Characteristics of Some Swept and Unswept Low-Aspect Ratio Wings. NACA TN 1468, 1947.

20. Nangia, R. K.: The Effects of Longitudinal Camber on Slender Wings. Ph.D. Dissertation, Univ. of London, 1967.

21. Marsden, D. J.; Simpson, R. W.; and Rainbird, B. E.: An Investigation into the Flow over Delta Wings at Low Speeds with Leading-Edge Separation. The College of Aeronautics (Cranfield), Report No. 114, 1958.

Table 1. Effect of number and type of wing panels on results for A = 2 arrow wing; $a/\ell = -0.273$, $\alpha = 25°$; M = 0.

Case Number	Number of Panels	Type of Paneling	C_L	C_D	$-C_M$	Σ (Residuals)^2	Number of Iterations
1*	30	Rows = 7 Columns = 6	1.154	0.538	0.145	0.115×10^{-4}	5
2	60	Rows = 13 Columns = 6	1.149	0.536	0.136	0.336×10^{-4}	5
3	60	Rows = 7 Columns = 11	No Convergence				10
4	--	Data (ref. 4)	1.1	0.5	0.02	---	-

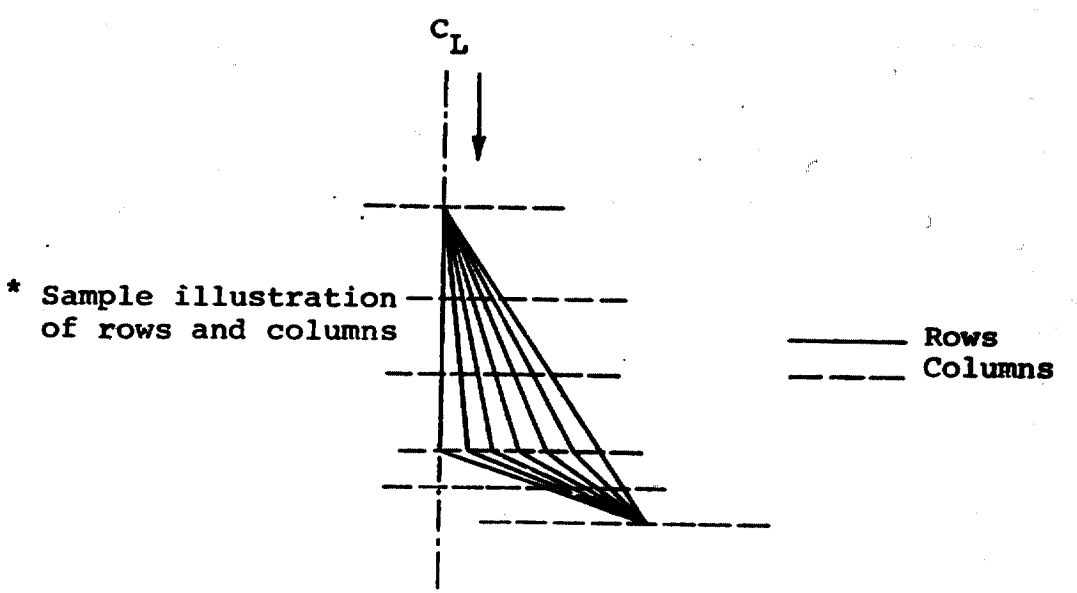

Table 2. Comparison of results obtained with and without design wake for A = 2 arrow wing; $a/\ell = -0.273$ $\alpha = 25°$; wing panels = 20; iterations = 5; M = 0.

Description	C_L	C_D	$-C_M$	Σ (Residuals)^2
with design wake	1.053	0.491	0.080	0.210×10^{-3}
without design wake	1.154	0.538	0.145	0.115×10^{-4}
data (ref. 4)	1.1	0.5	0.02	-

Table 3. Wing configurations modeled using free vortex sheet method (ref. 2); M = 0.

Serial Number	Wing Description	Aspect Ratio	Range of Angle of Attack	Number of Panels	Solution Converged?
			FLAT WINGS		
1	76° delta	1.00	5 - 30°	30	Yes
2(a)	70° delta	1.46	5°	30	No
2(b)	70° delta	1.46	10 - 40°	30	Yes
3	45° delta	4.00	10.36°	30	No
4	45° cropped delta	1.33	20.83°	42,48	No
5	70° arrow, $a/\ell = -0.273$	2.00	15 - 40°	30,60	Yes
6	70° arrow, $a/\ell = -0.20$	1.82	15 - 40°	30	Yes
7	70° arrow, $a/\ell = -0.10$	1.62	15 - 40°	30	Yes
8	70° diamond, $a/\ell = 0.10$	1.32	15 - 40°	30,48	Yes
9	70° diamond, $a/\ell = 0.20$	1.21	15 - 40°	30	Yes
10	70° diamond, $a/\ell = 0.30$	1.12	15 - 40°	30	Yes
11	70° diamond, $a/\ell = 0.40$	1.04	15 - 40°	30	Yes
12	70° diamond, $a/\ell = 0.455$	1.00	15 - 40°	30	Yes

(Cont'd)

Table 3. Wing configurations modeled using free vortex sheet method (ref. 2); M = 0. (Concluded)

Serial Number	Wing Description	Aspect Ratio	Range of Angle of Attack	Number of Panels	Solution Converged?
		SPANWISE CAMBERED WINGS			
13	76° delta, 5% camber	1.0	10 - 30°	30	Yes
14	76° deltas 1-4 (ref. 3)	1.0	10 - 40°	48	Yes
15(a)	76° delta 5 (ref. 3)	1.0	10 - 20°	48	No
15(b)	76° delta 5 (ref. 3)	1.0	30 - 40°	48	Yes
16	76° deltas 6,7 (ref. 3)	1.0	10 - 40°	48	No

Table 4. Wing configurations modeled using quasi-vortex lattice method (ref. 11); M = 0.

Serial Number	Wing Description	Aspect Ratio	Range of Angle of Attack	Solution Converged?
		FLAT WINGS		
1	76° delta	1.0	15°	Yes
2	70° delta	1.46	14°	Yes
3	45° delta	4.0	10.36°	No
4	70° arrow, a/ℓ = -0.273	2.0	15 - 40°	Yes
5	70° diamond, a/ℓ = 0.455	1.0	15 - 40°	Yes
		SPANWISE CAMBERED WINGS		
6	70° delta, 5% camber	1.0	15 - 30°	Yes
7	76° deltas 2-4 (ref. 3)	1.0	10 - 30°	Yes

Table 5. Wing configurations modeled using suction analogy method (ref. 15); M = 0; range of angle of attack = -10° to 40°.

Serial Number	Wing Description	Aspect Ratio
	FLAT WINGS	
1	76° delta	1.00
2	70° delta	1.46
3	70° arrow. a/ℓ = -0.273	2.00
4	70° arrow, a/ℓ = -0.20	1.82
5	70° arrow, a/ℓ = -0.10	1.62
6	70° diamond, a/ℓ = 0.10	1.32
7	70° diamond, a/ℓ = 0.20	1.21
8	70° diamond, a/ℓ = 0.30	1.12
9	70° diamond, a/ℓ = 0.40	1.04
10	70° diamond, a/ℓ = 0.455	1.00
	SPANWISE CAMBERED WINGS	
11	76° delta, 5% camber	1.00
12	76° deltas 1-7 (ref.3)	1.00

Table 6. Constants for Squire's wings (ref. 3).

Wing	n	β	ε
1	-	0.0	0.25
2	2	0.15	0.25
3	5	0.15	0.25
4	1	0.30	0.25
5	3	0.30	0.25
6	5	0.30	0.25
7	7	0.30	0.25

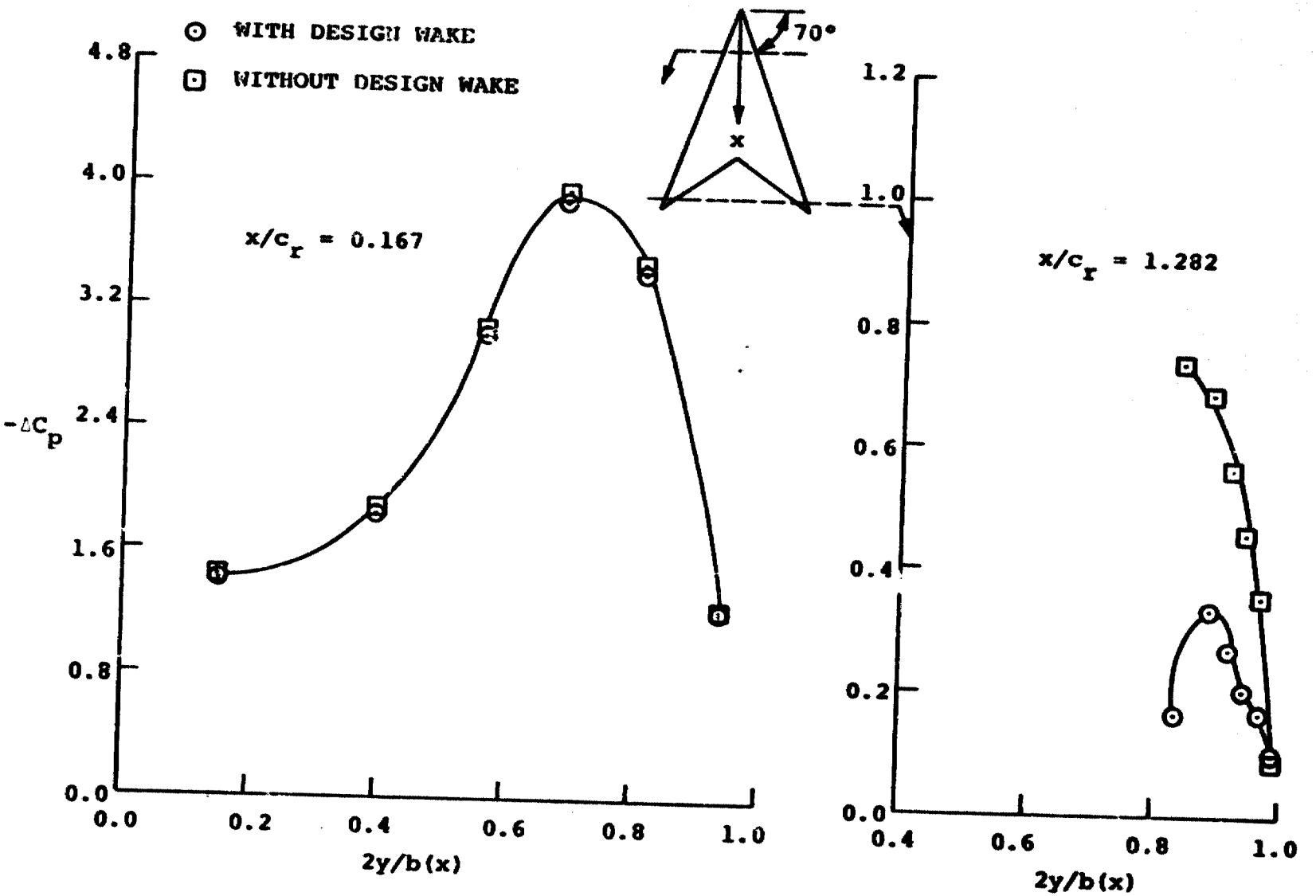

Figure 1. Effect of design wake on spanwise pressure distribution for A = 2 arrow wing; a/ℓ = -0.273; α = 25°; M = 0.

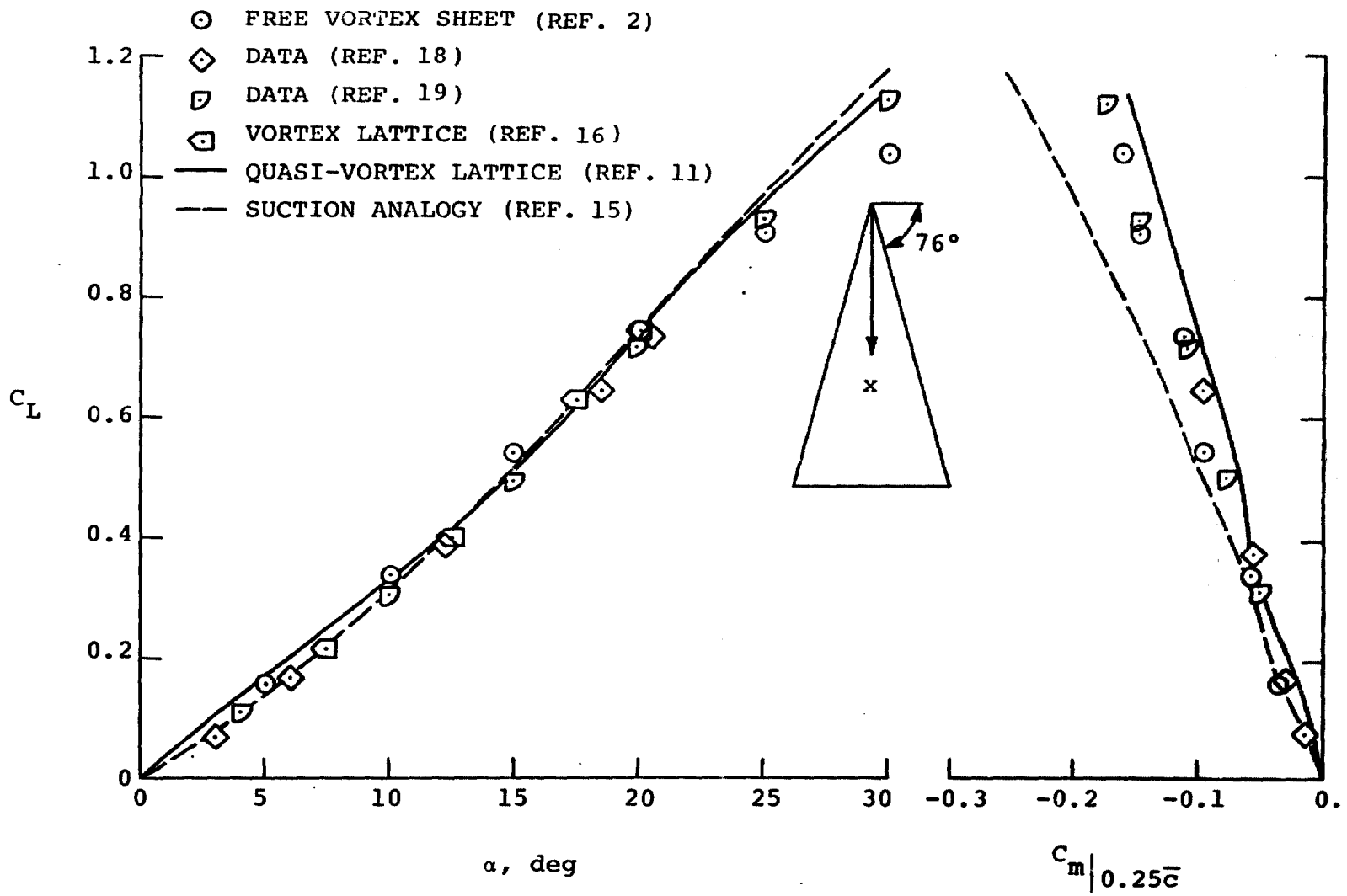

Figure 2. Longitudinal aerodynamic characteristics of A = 1 delta wing; M ≈ 0.

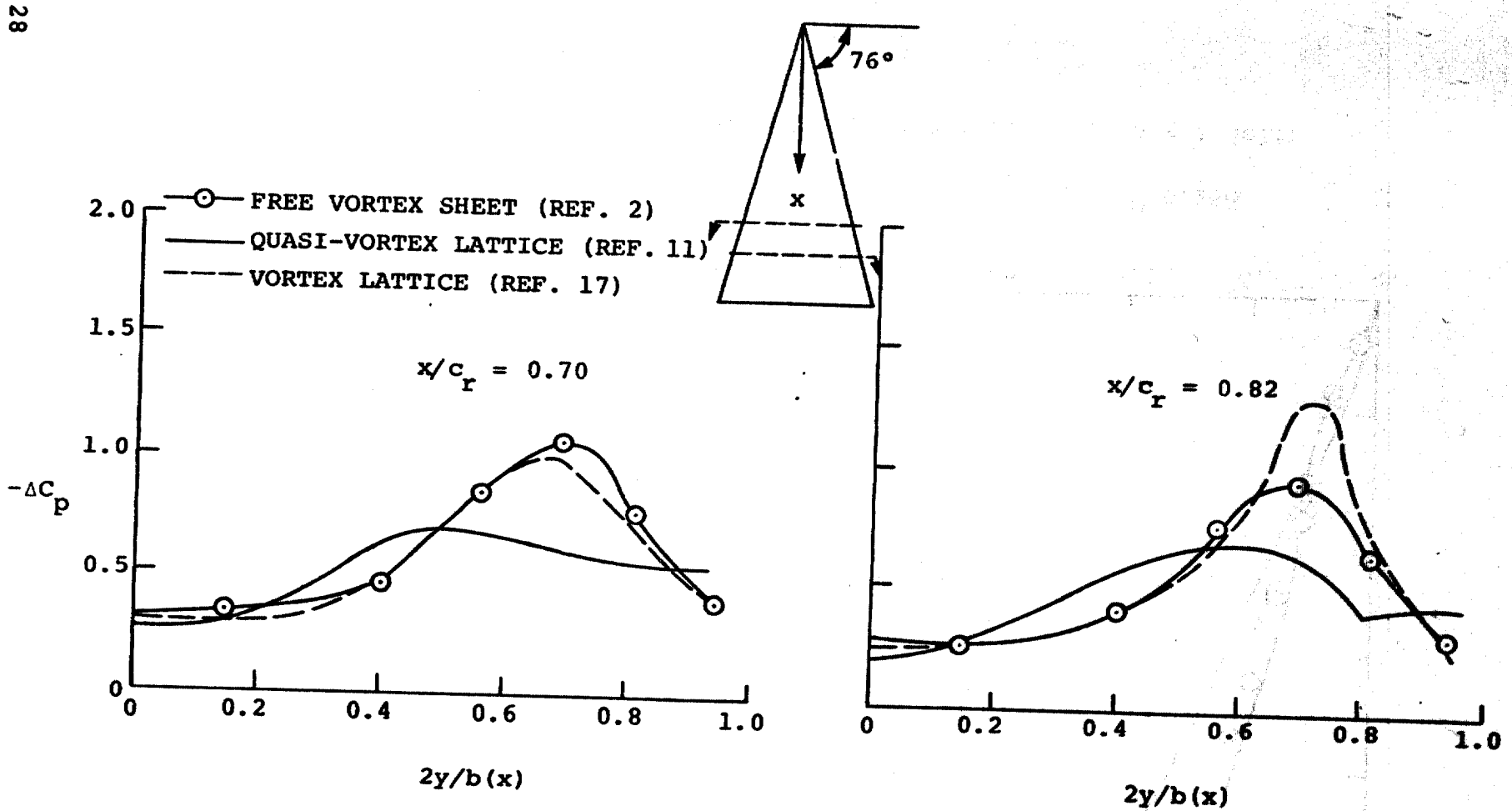

Figure 3. Theoretical spanwise pressure distributions for A = 1 delta wing; $\alpha = 15°$; M = 0.

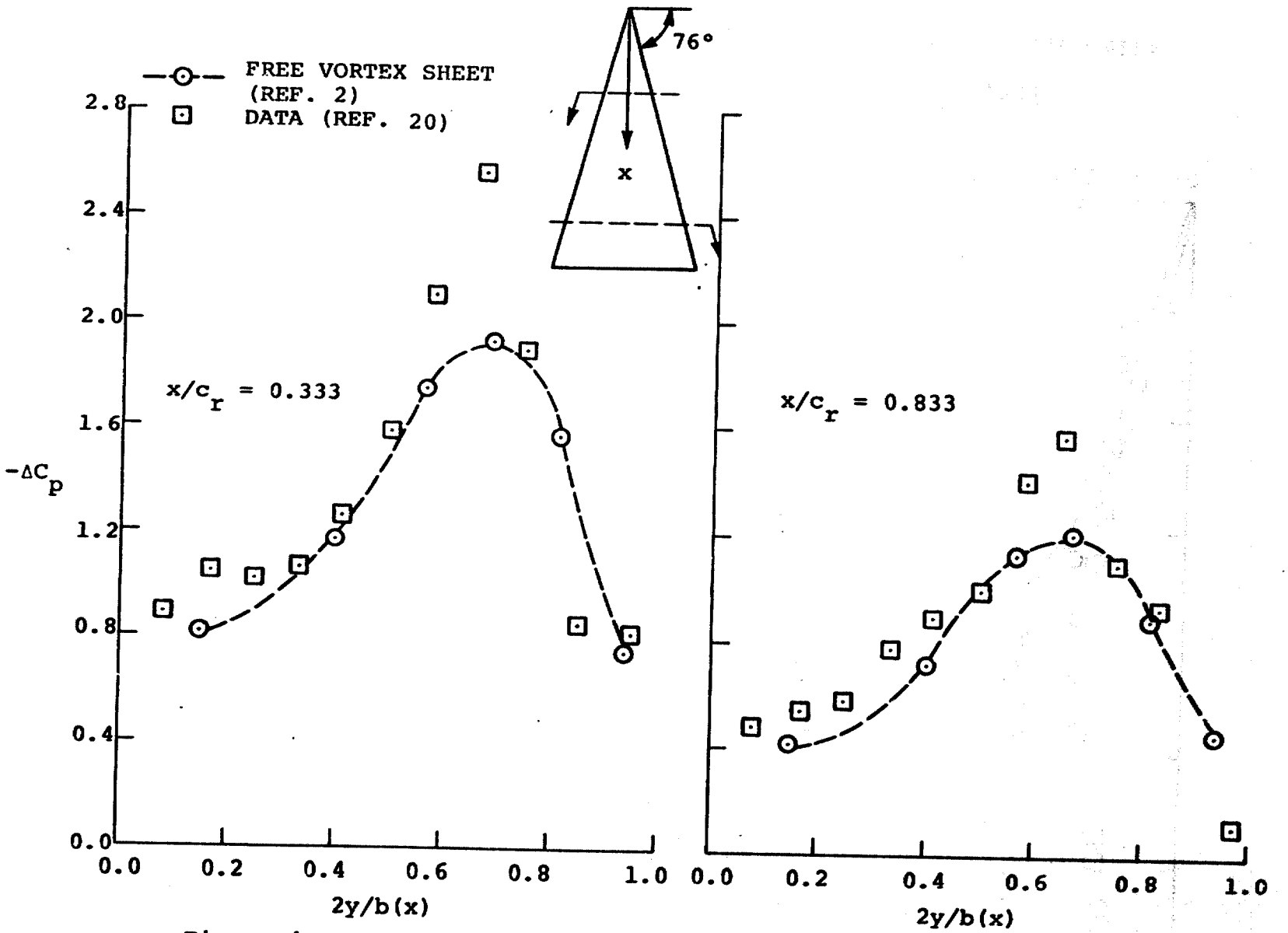

Figure 4. Spanwise pressure distributions for A = 1 delta wing; $\alpha = 22.5°$; $M \approx 0$.

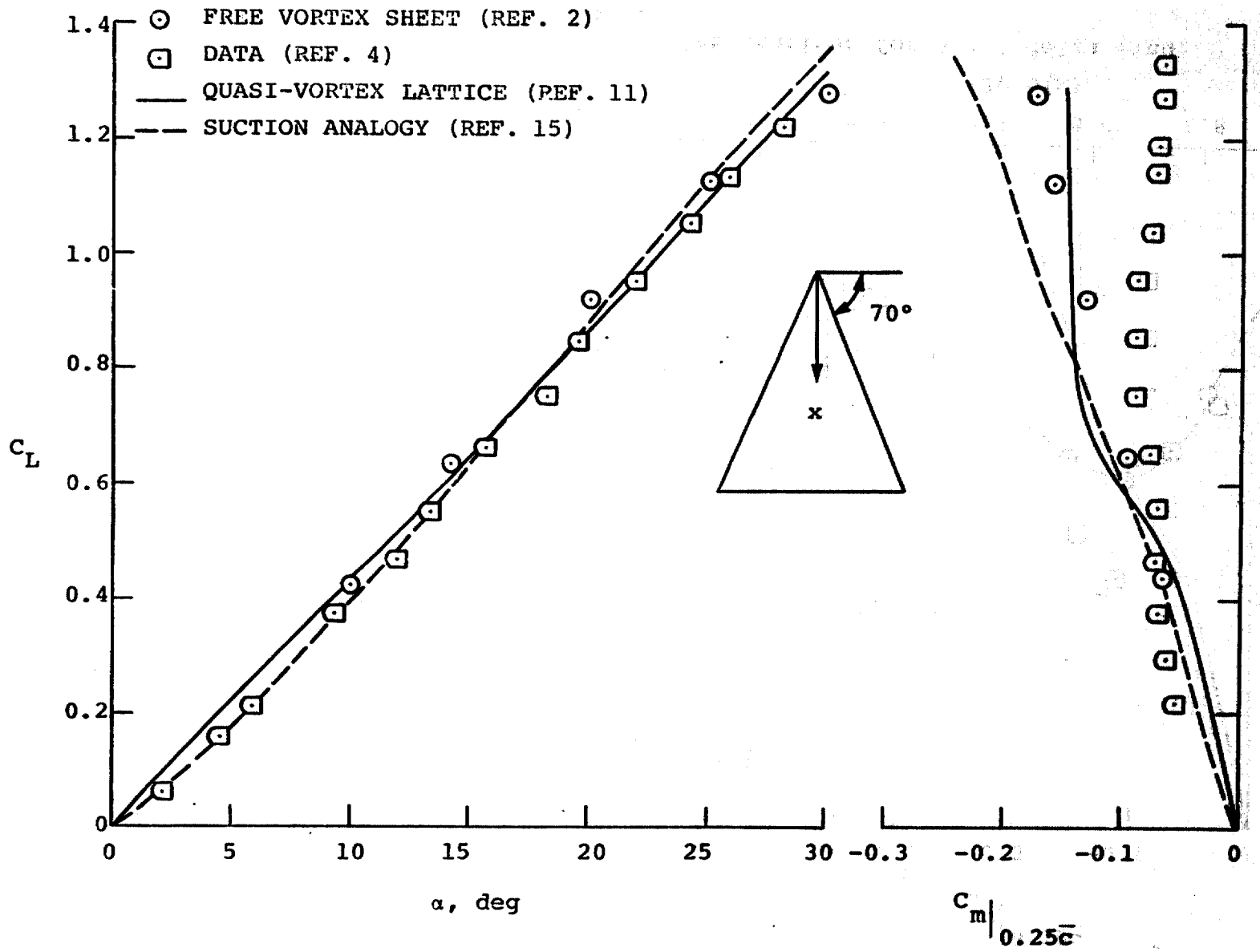

Figure 5. Longitudinal aerodynamic characteristics of A = 1.46 delta wing; M ≈ 0.

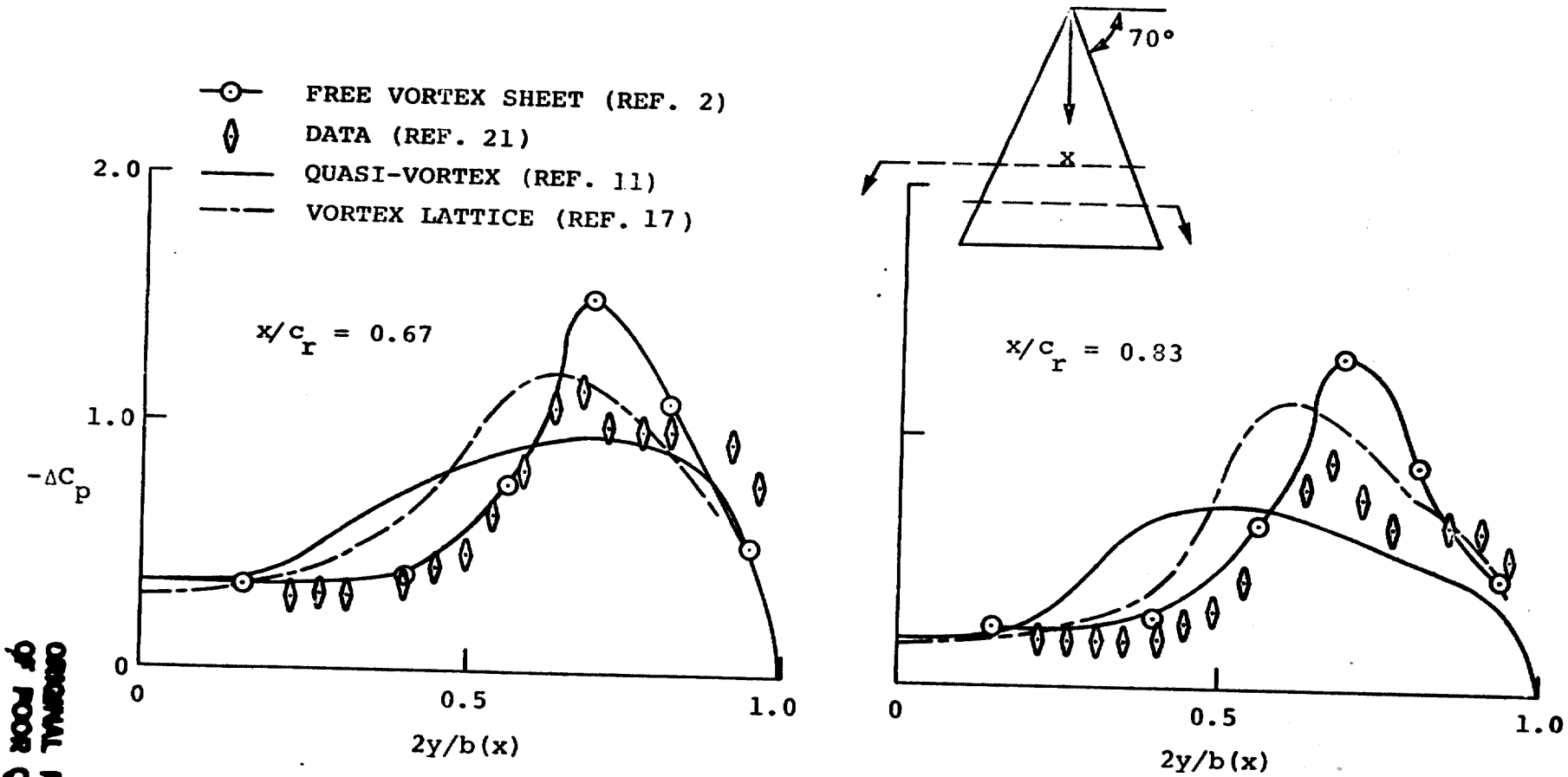

Figure 6. Spanwise pressure distributions for A = 1.46 delta wing; $\alpha = 14°$; $M \approx 0$.

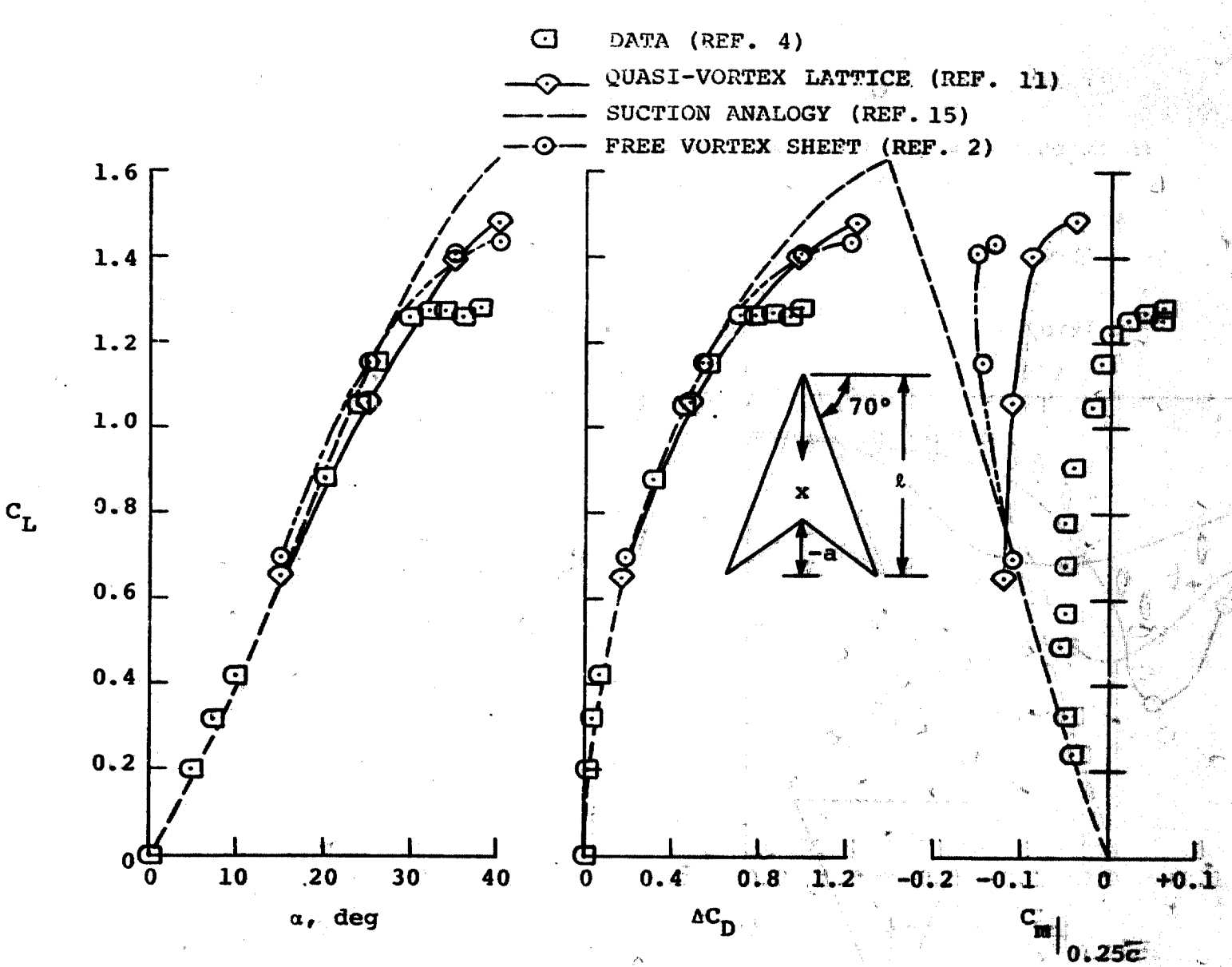

Figure 7. Longitudinal aerodynamic characteristics of A = 2 arrow wing; $a/\ell = -0.273$; $M \approx 0$.

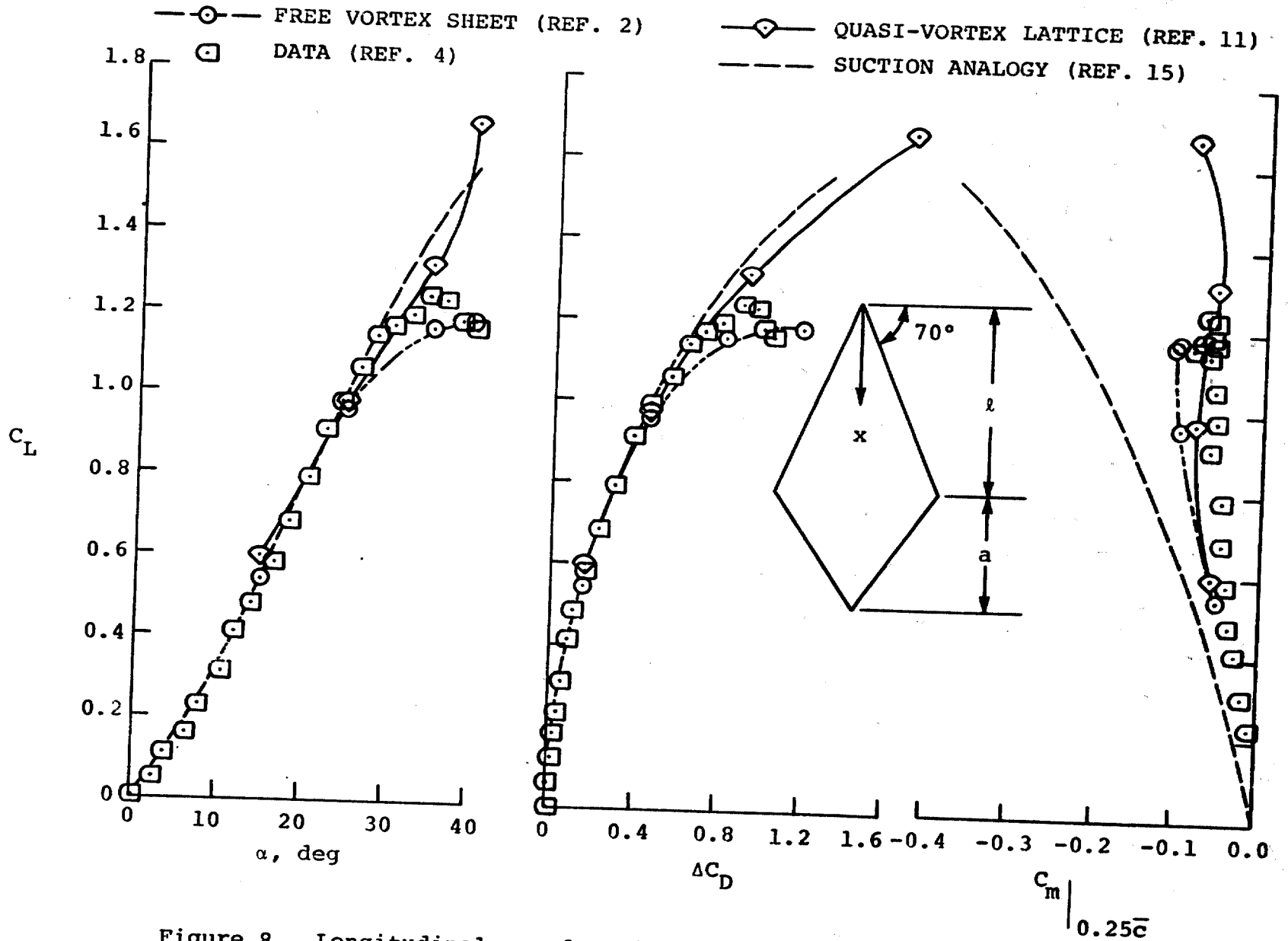

Figure 8. Longitudinal aerodynamic characteristics for A = 1 diamond wing; $a/\ell = 0.455$; $M \approx 0$.

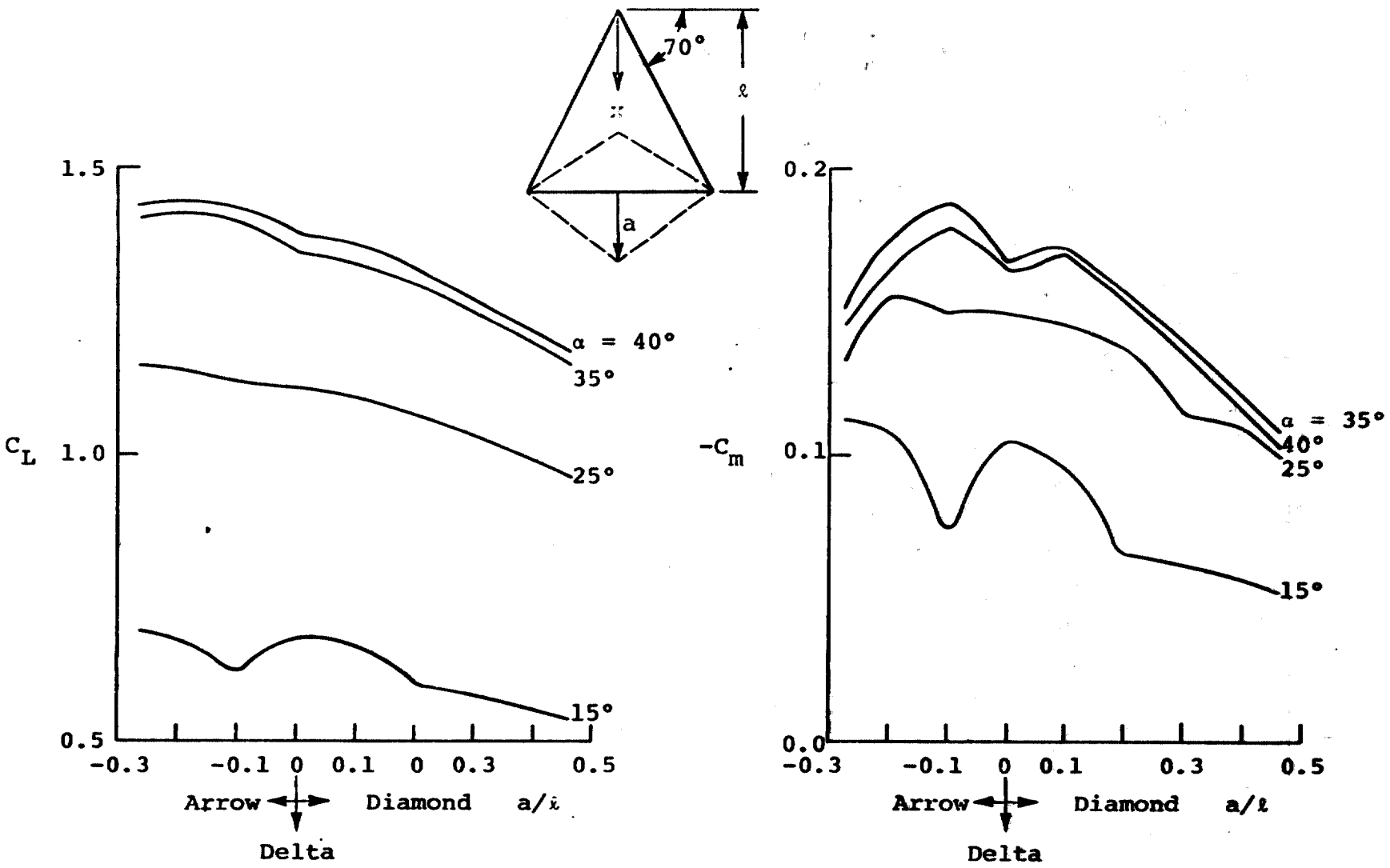

Figure 9. Effect of angle of attack on longitudinal aerodynamic characteristics of pointed wings at various notch ratios by free vortex sheet method; M = 0 (ref. 2).

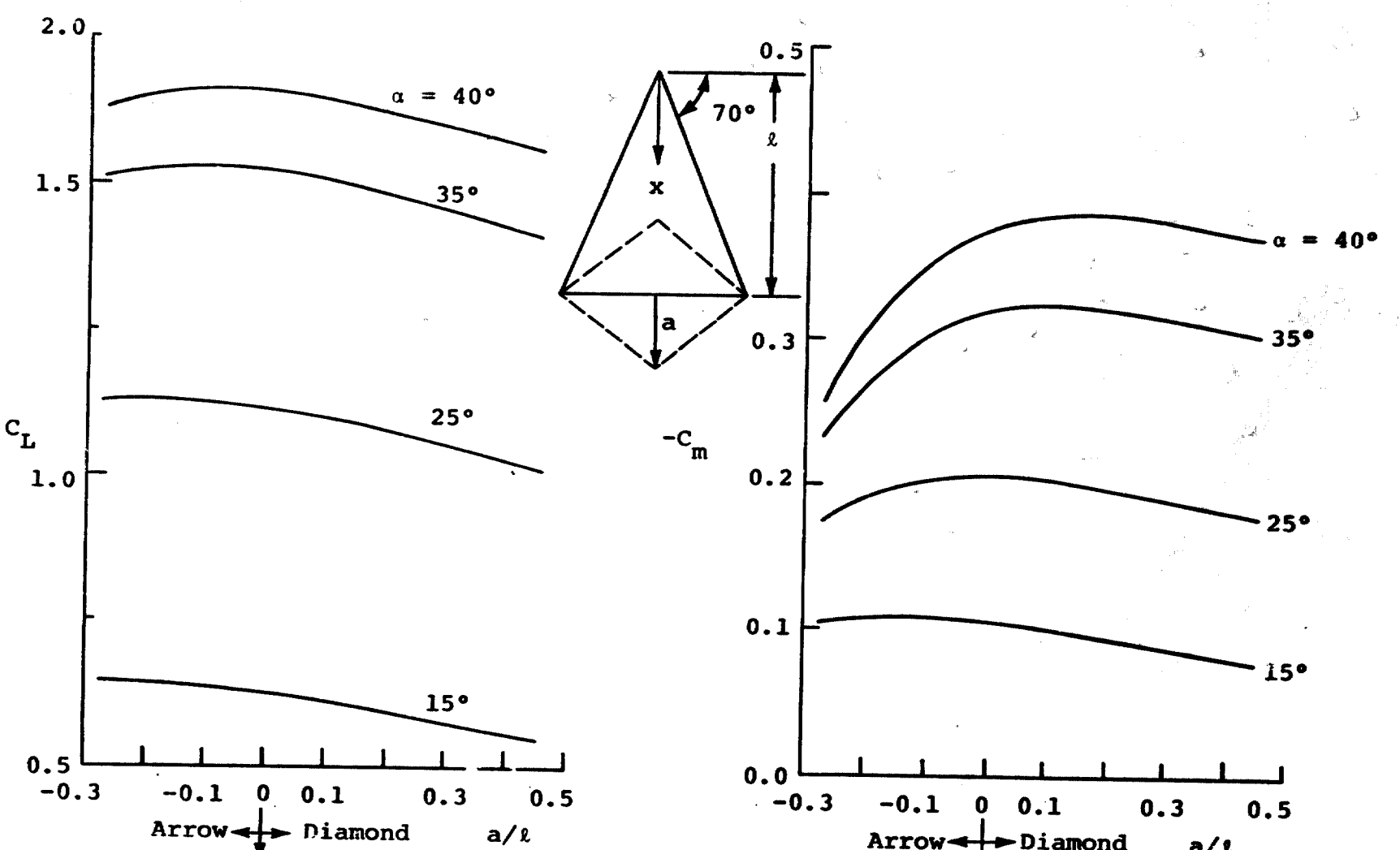

Figure 10. Effect of angle of attack on longitudinal aerodynamic characteristics of pointed wings of various notch ratios by suction analogy method; M = 0 (ref. 15).

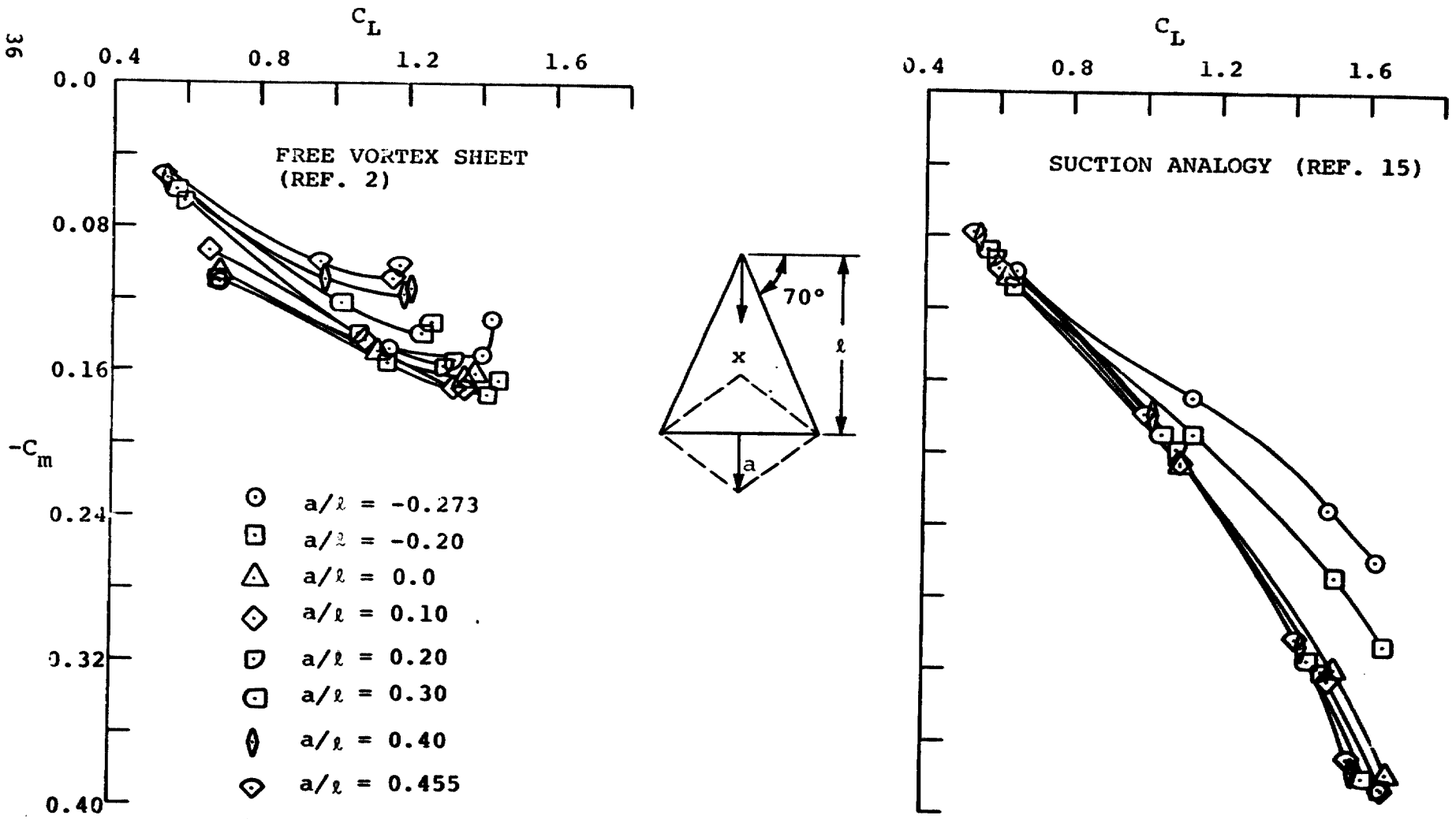

Figure 11. Theoretical estimates of longitudinal stability variation for wings with trailing edge notch; M = 0.

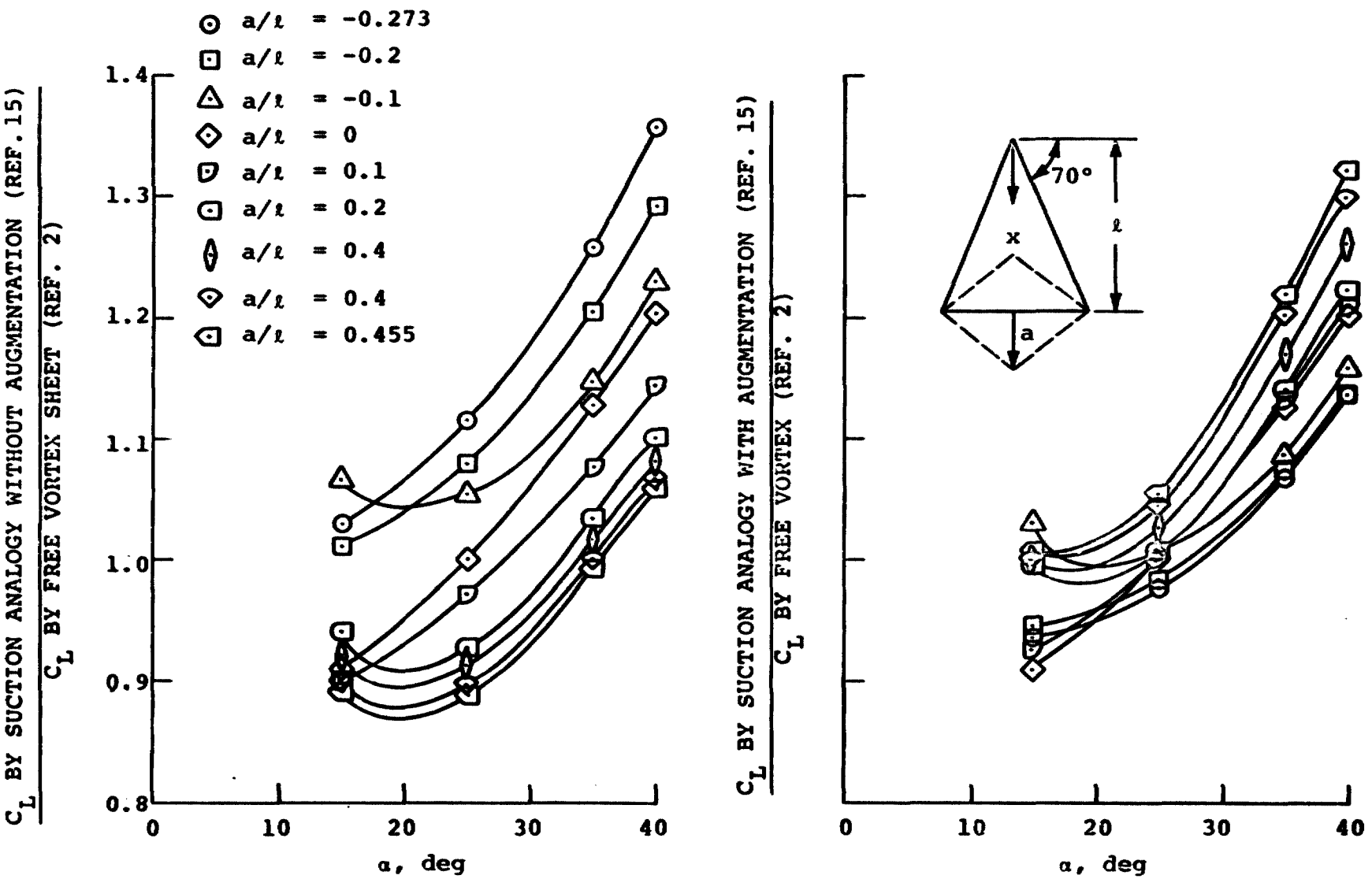

Figure 12. Lift coefficient characteristics for wings with trailing edge notch; M = 0.

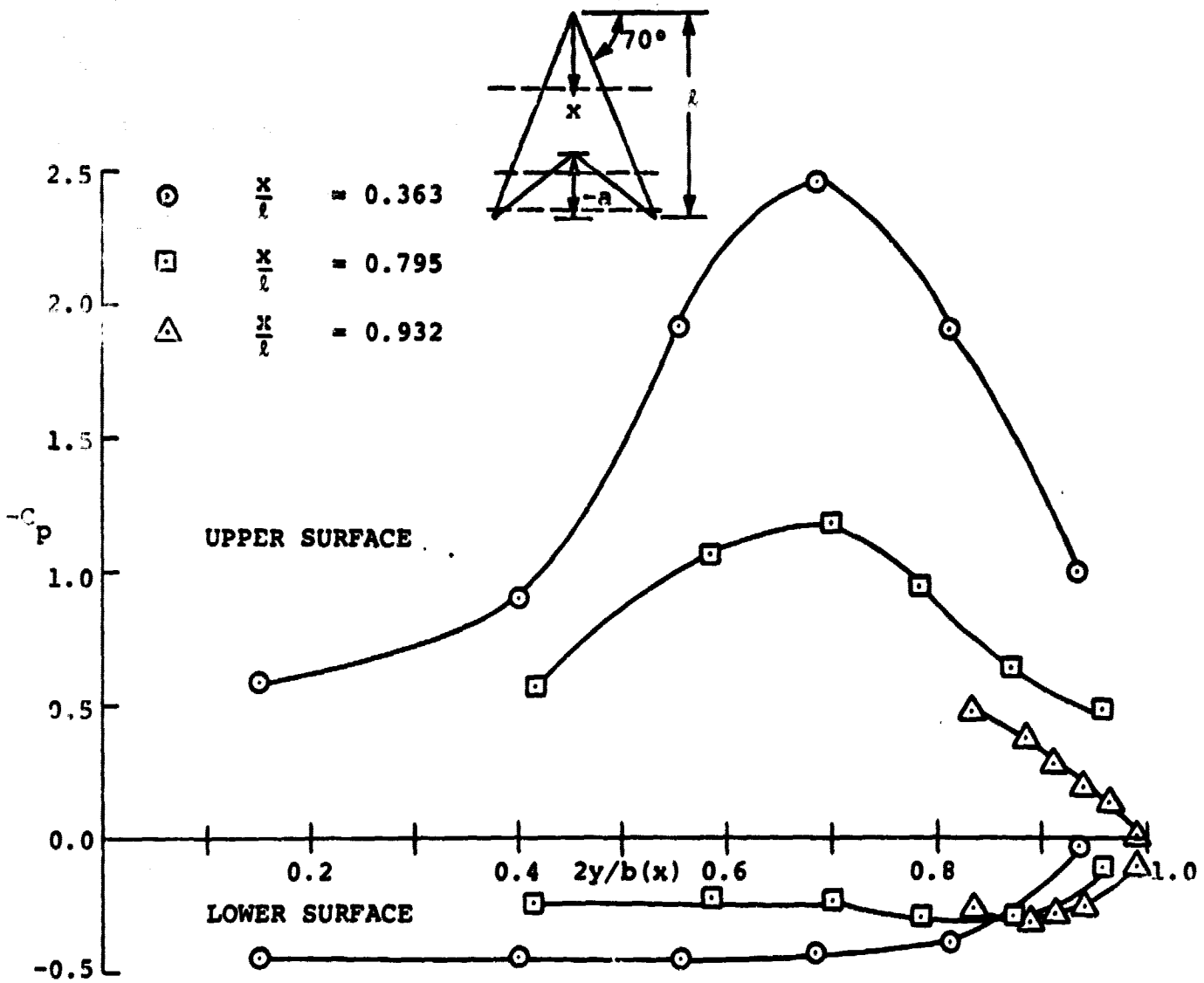

Figure 13. Spanwise pressure distributions for A = 2 arrow wing; a/ℓ = -0.273; α = 25°; M = 0.

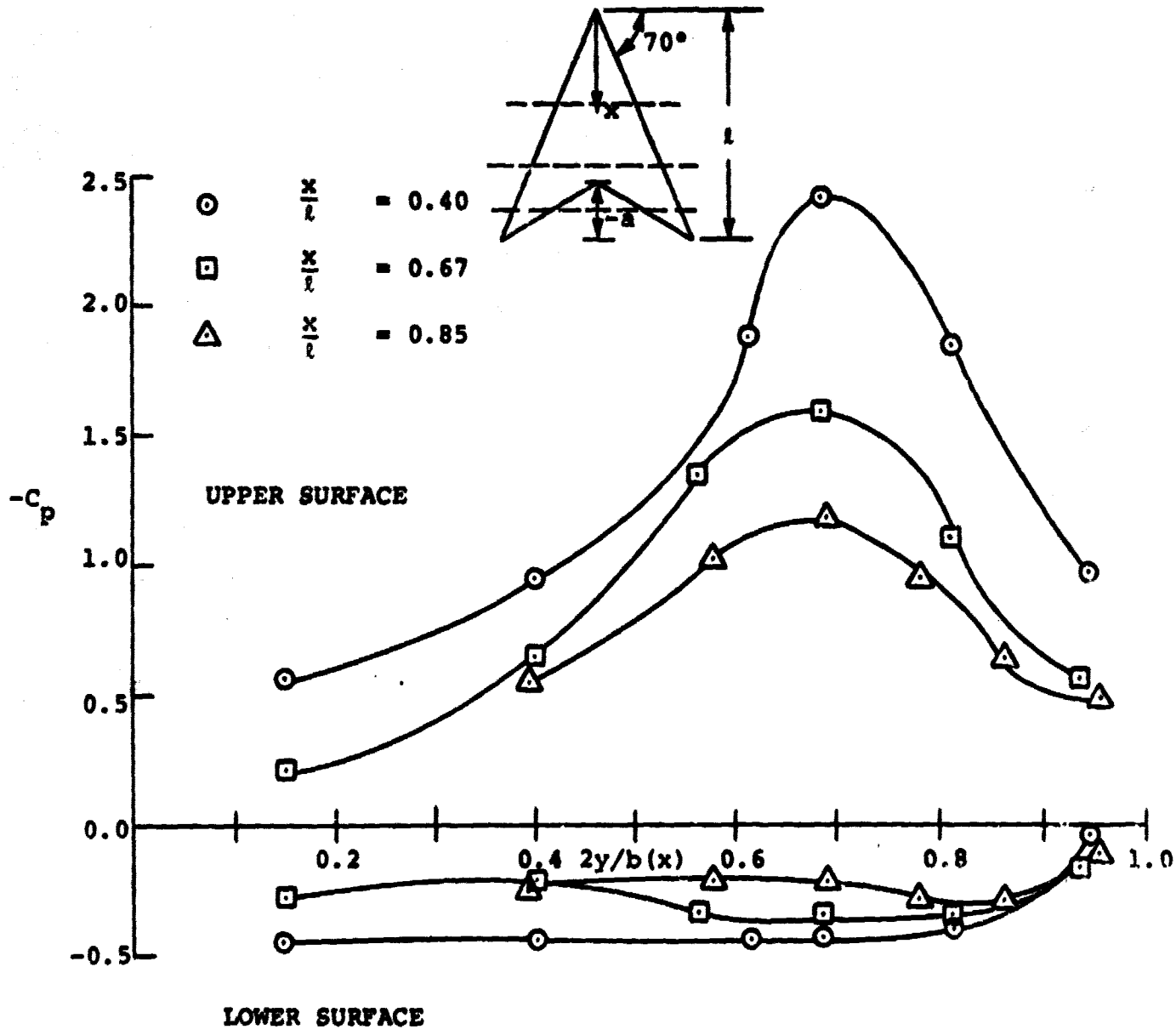

Figure 14. Spanwise pressure distributions for A = 1.82 arrow wing; a/ℓ = -0.2; α = 25°; M =0.

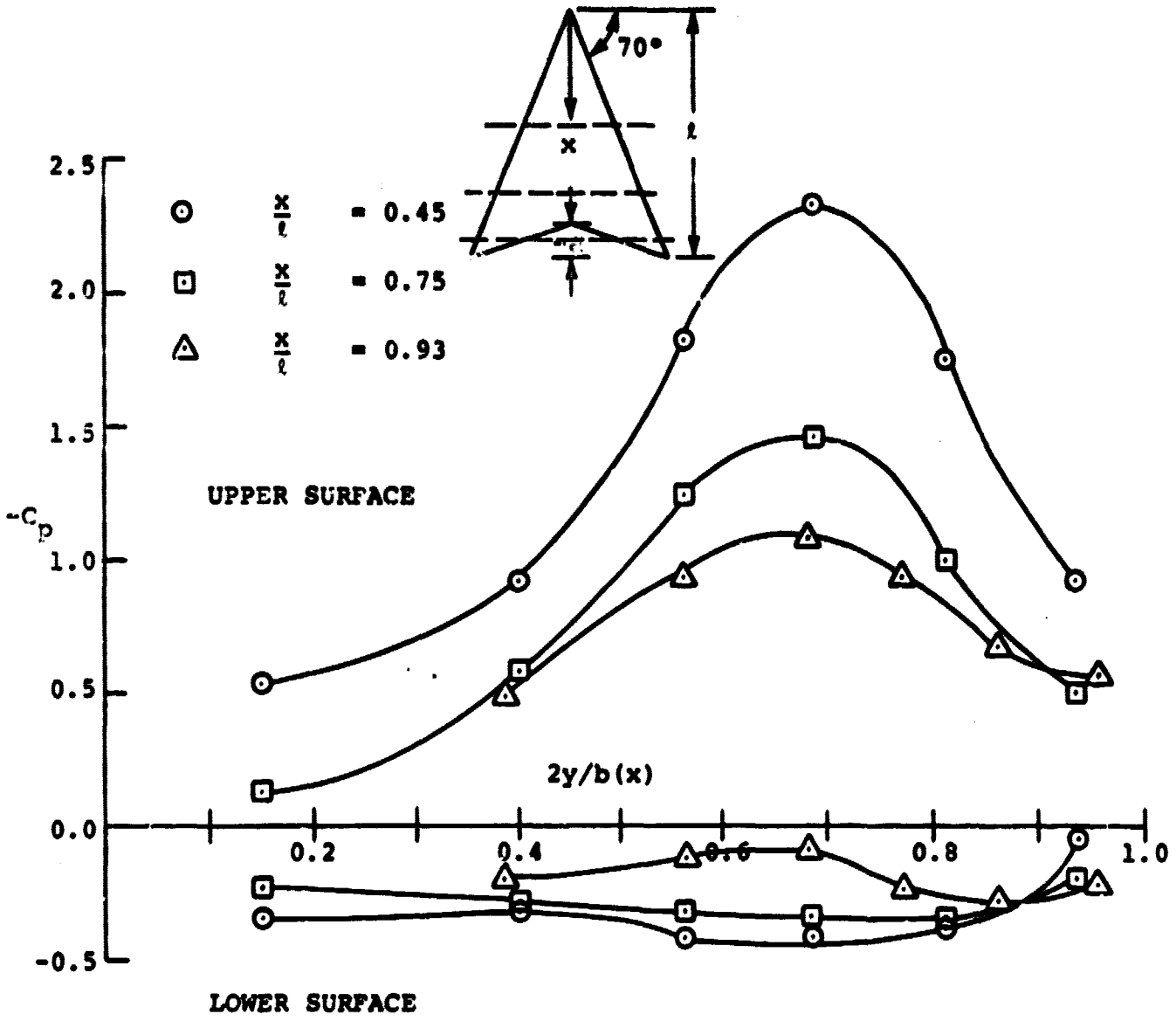

Figure I5. Spanwise pressure distributions for A = 1.62 arrow wing; a/ℓ = -0.1; α = 25°, M = 0.

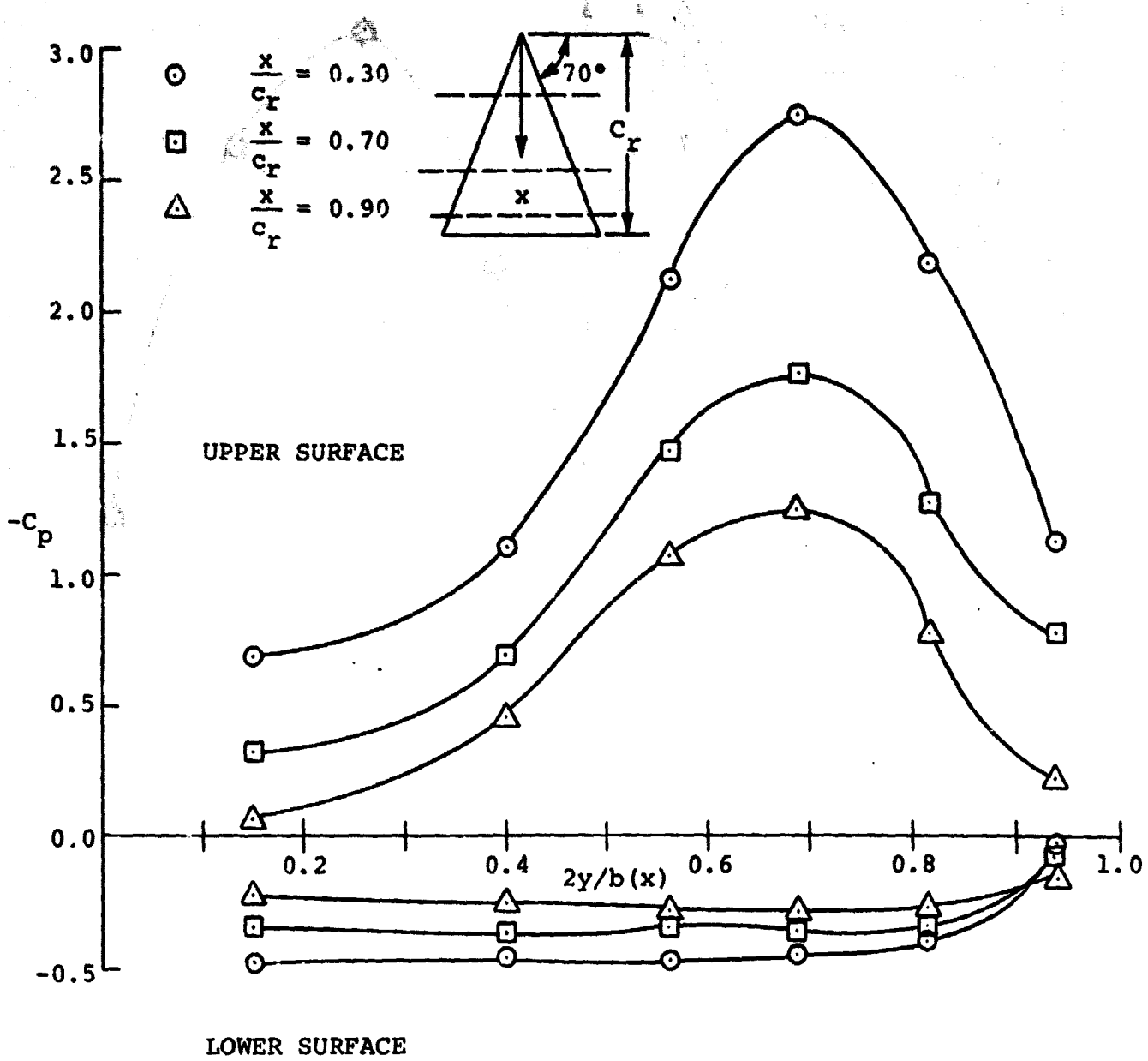

Figure 16. Spanwise pressure distributions for A = 1.46 delta wing; α = 25°; M = 0.

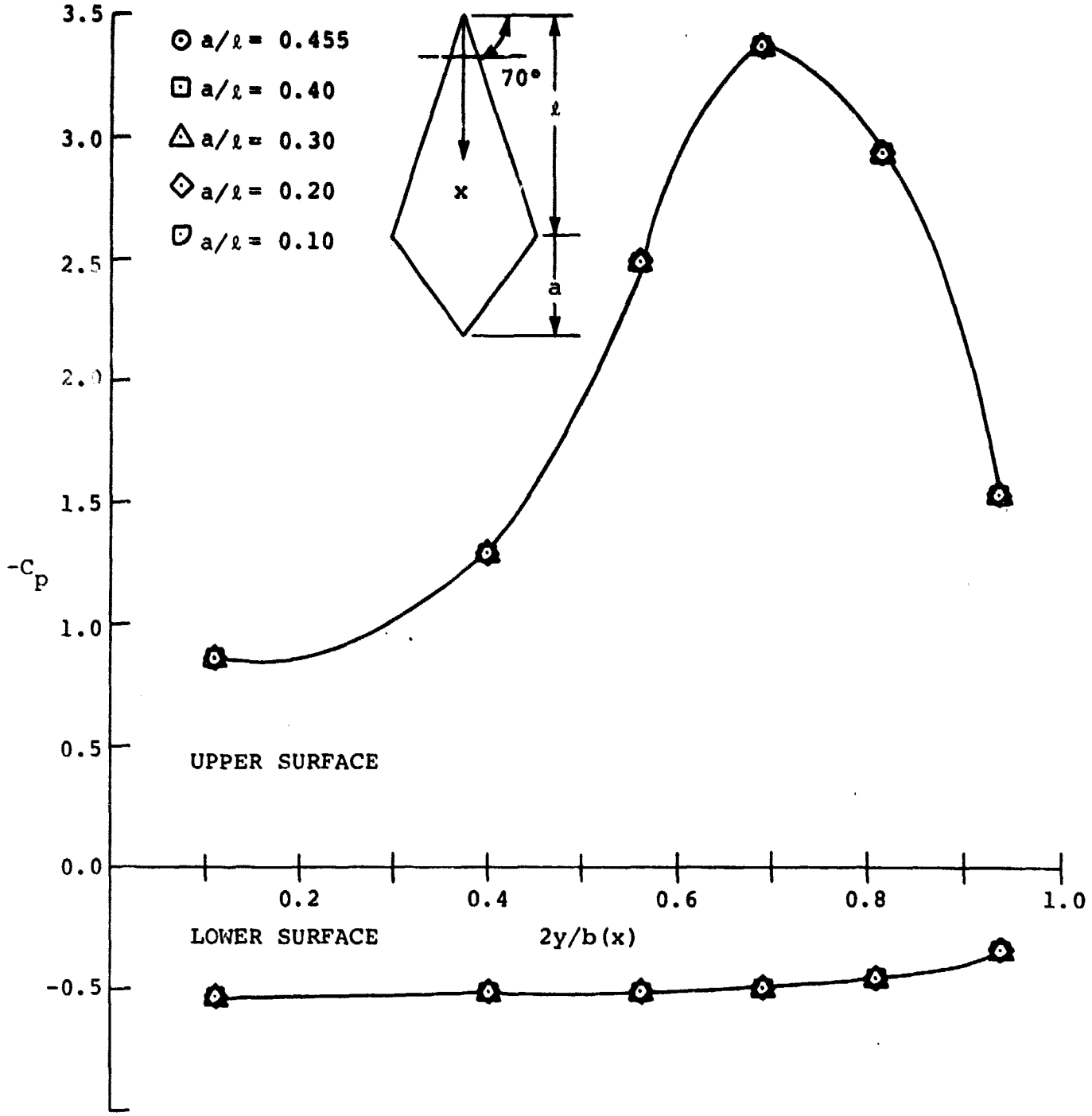

Figure 17. Effect of notch ratio on spanwise pressure distributions for 70° diamond wings at $x/\ell = 0.167$; $\alpha = 25°$; $M = 0$.

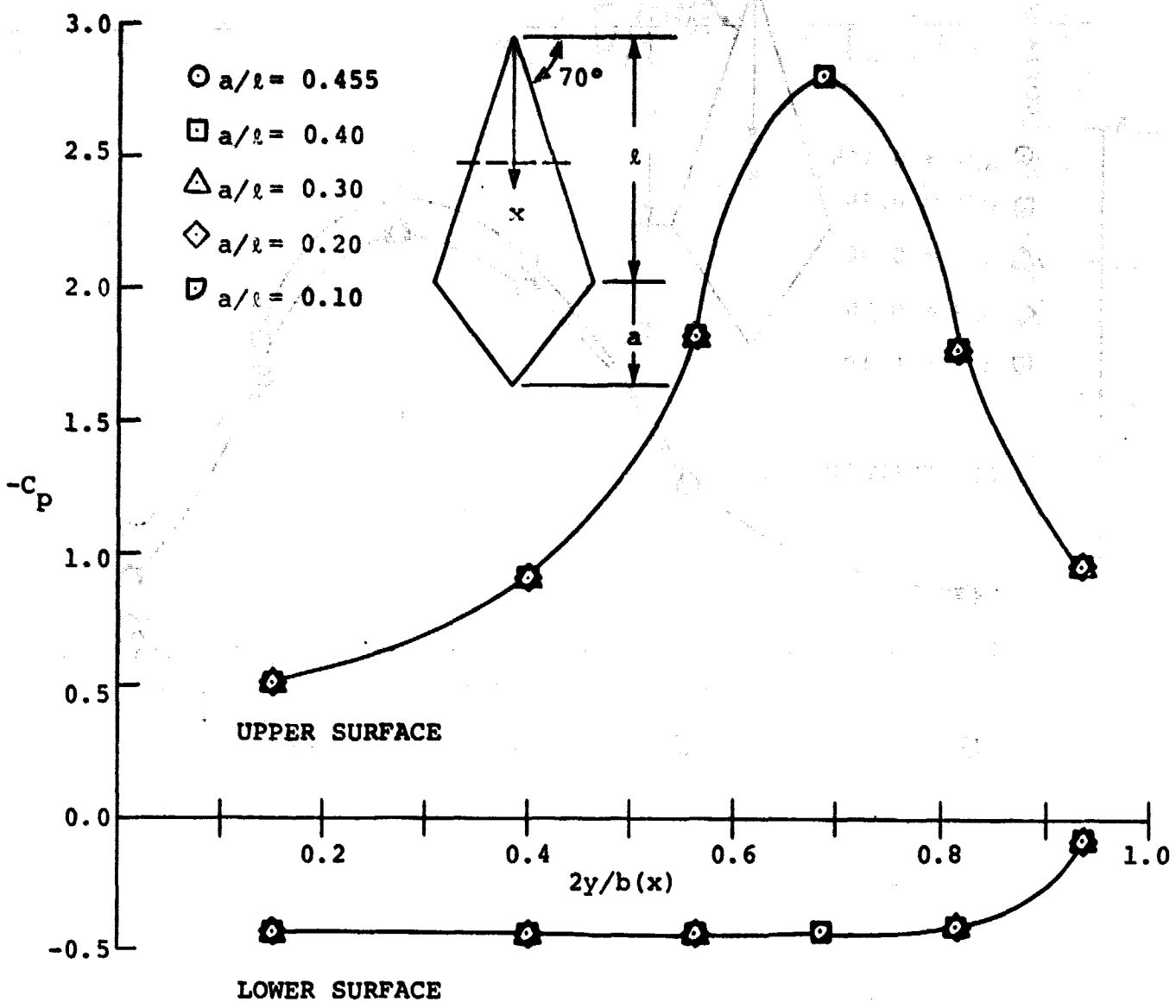

Figure 18. Effect of notch ratio on spanwise pressure distributions for 70° diamond wings as $x/\ell = 0.50$; $\alpha = 25°$; $M = 0$.

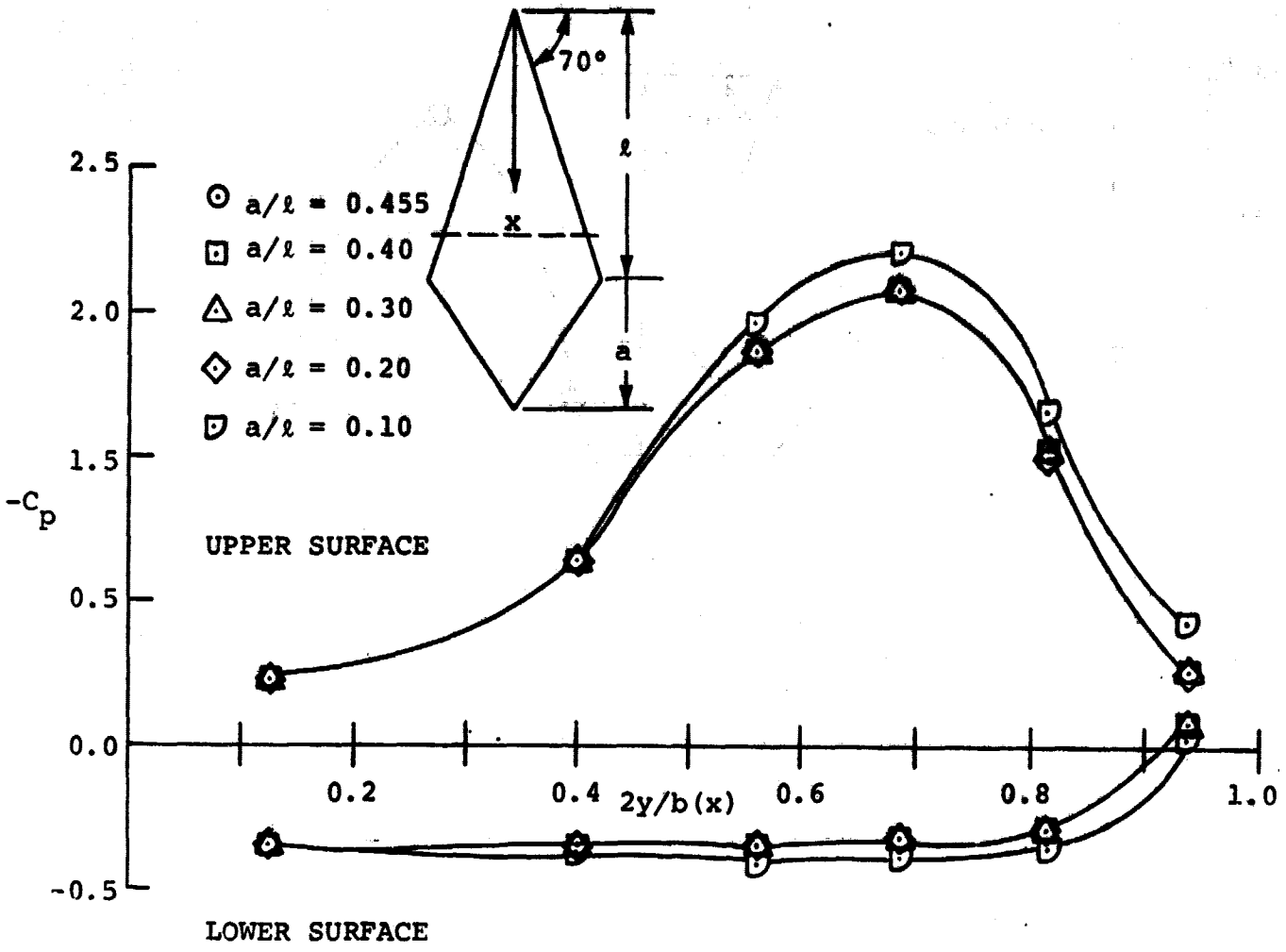

Figure 19. Effect of notch ratio on spanwise pressure distributions for 70° diamond wings at $x/\ell = 0.833$; $\alpha = 25°$; $M = 0$.

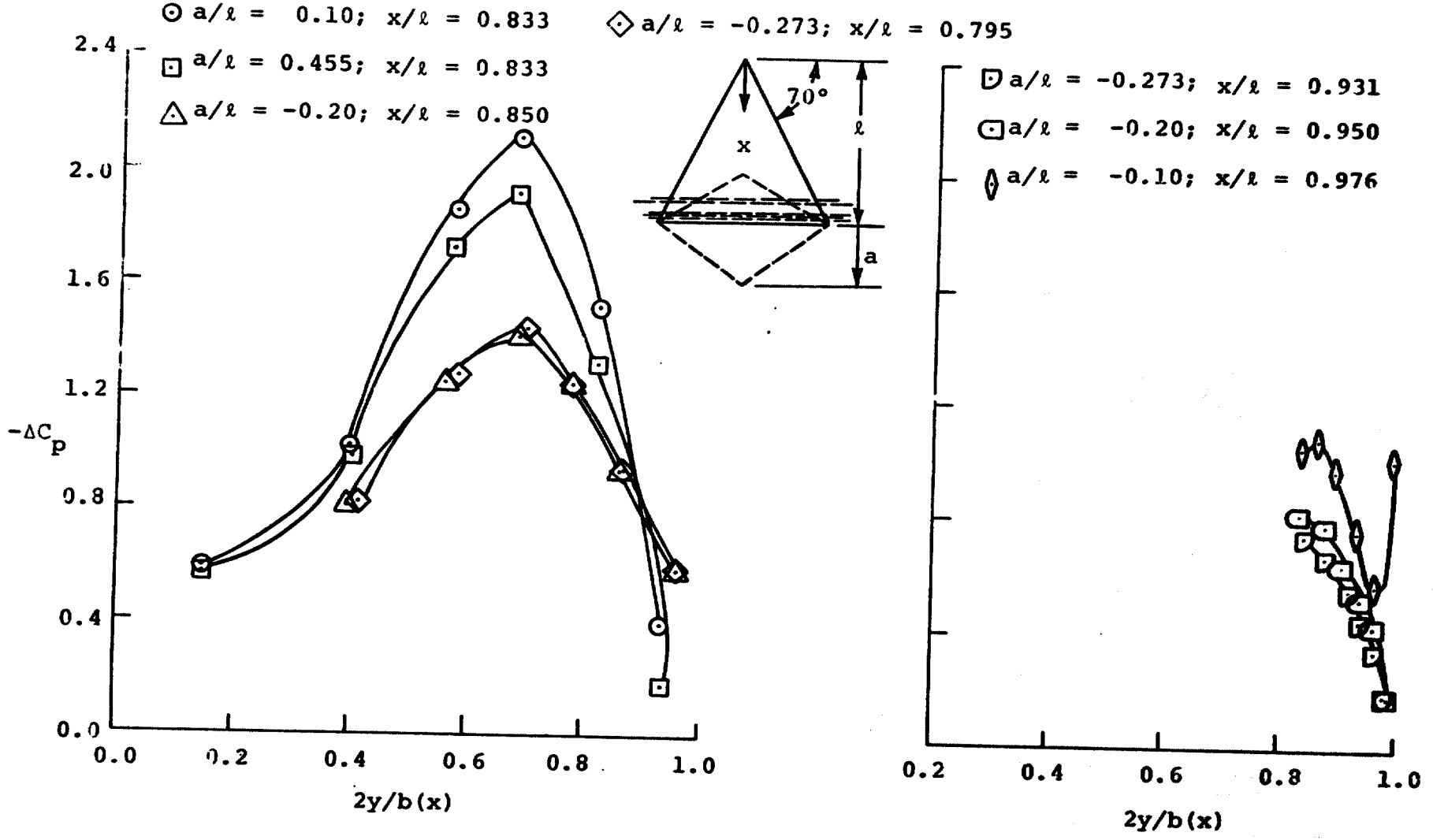

Figure 20. Spanwise pressure distributions near the trailing edge for family of arrow and diamond wings; $\alpha = 25°$; $M = 0$.

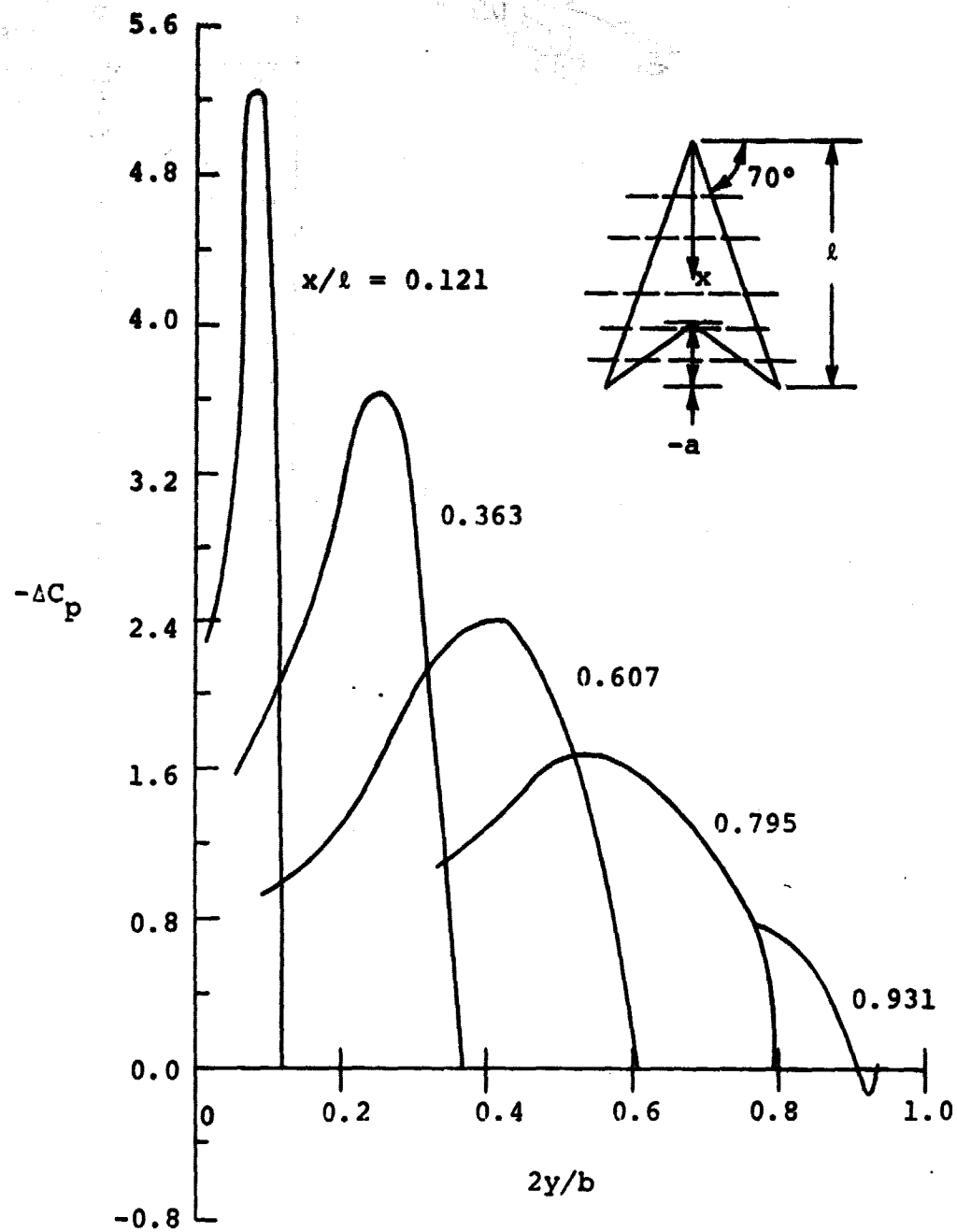

Figure 21. Spanwise pressure distributions at various chordwise stations for A = 2 arrow wing; $a/\ell = -0.273$; $\alpha = 35°$; M = 0.

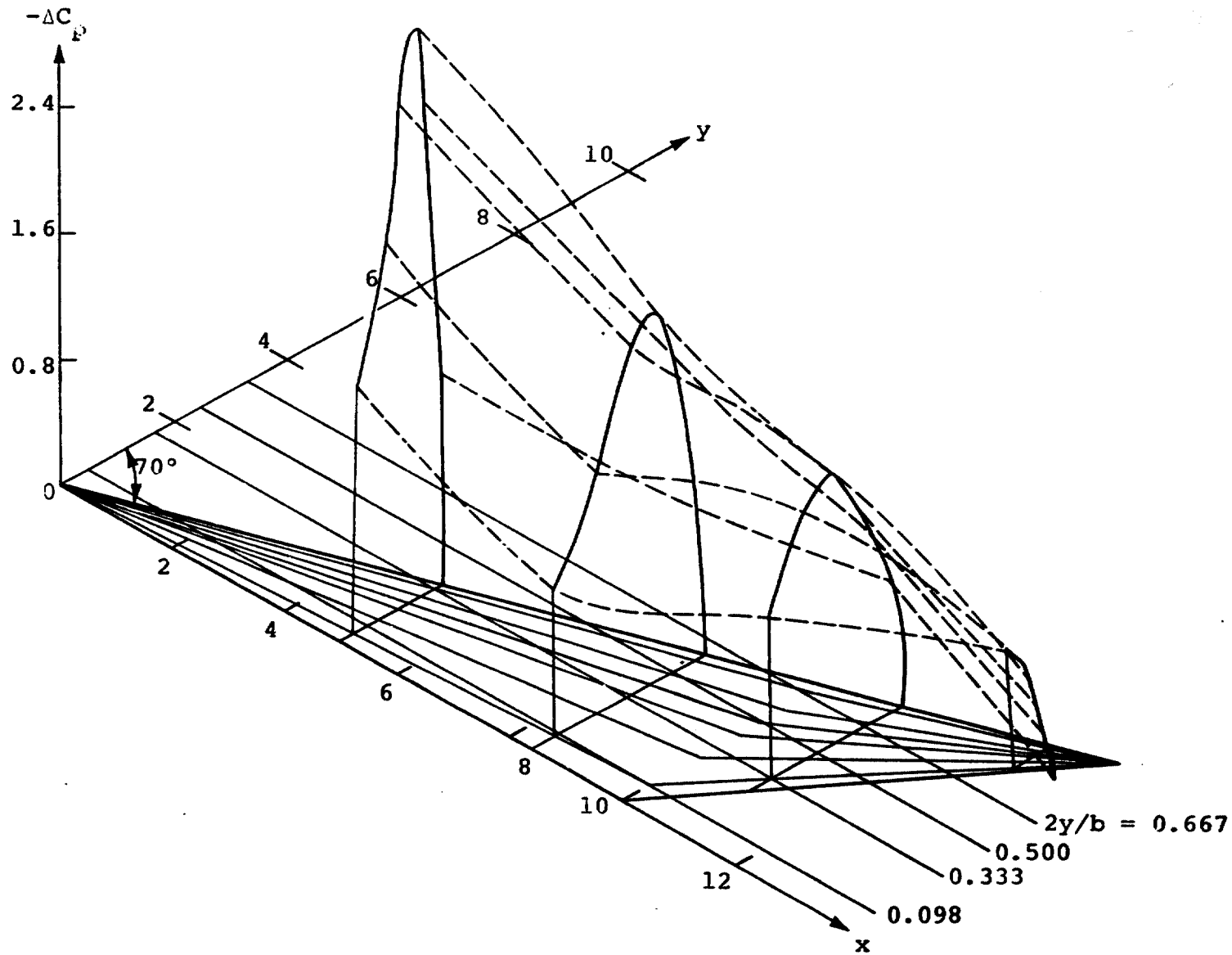

Figure 22. Surface pressure distribution on A = 2 arrow wing; $a/\ell = -0.273$; $\alpha = 35°$; M = 0.

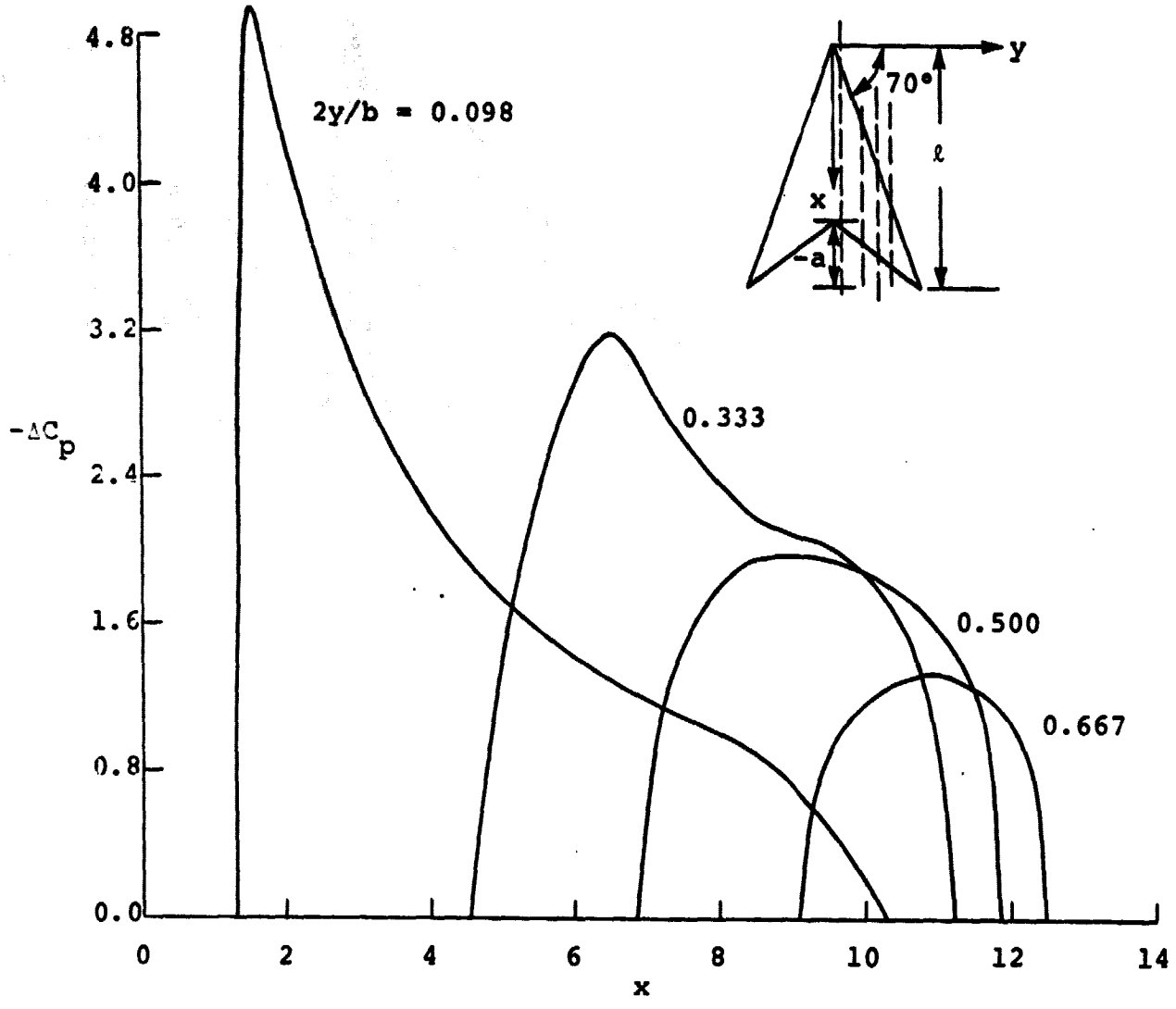

Figure 23. Chordwise pressure distributions for A = 2 arrow wing; $a/\ell = -0.273$; $\alpha = 35°$; M = 0.

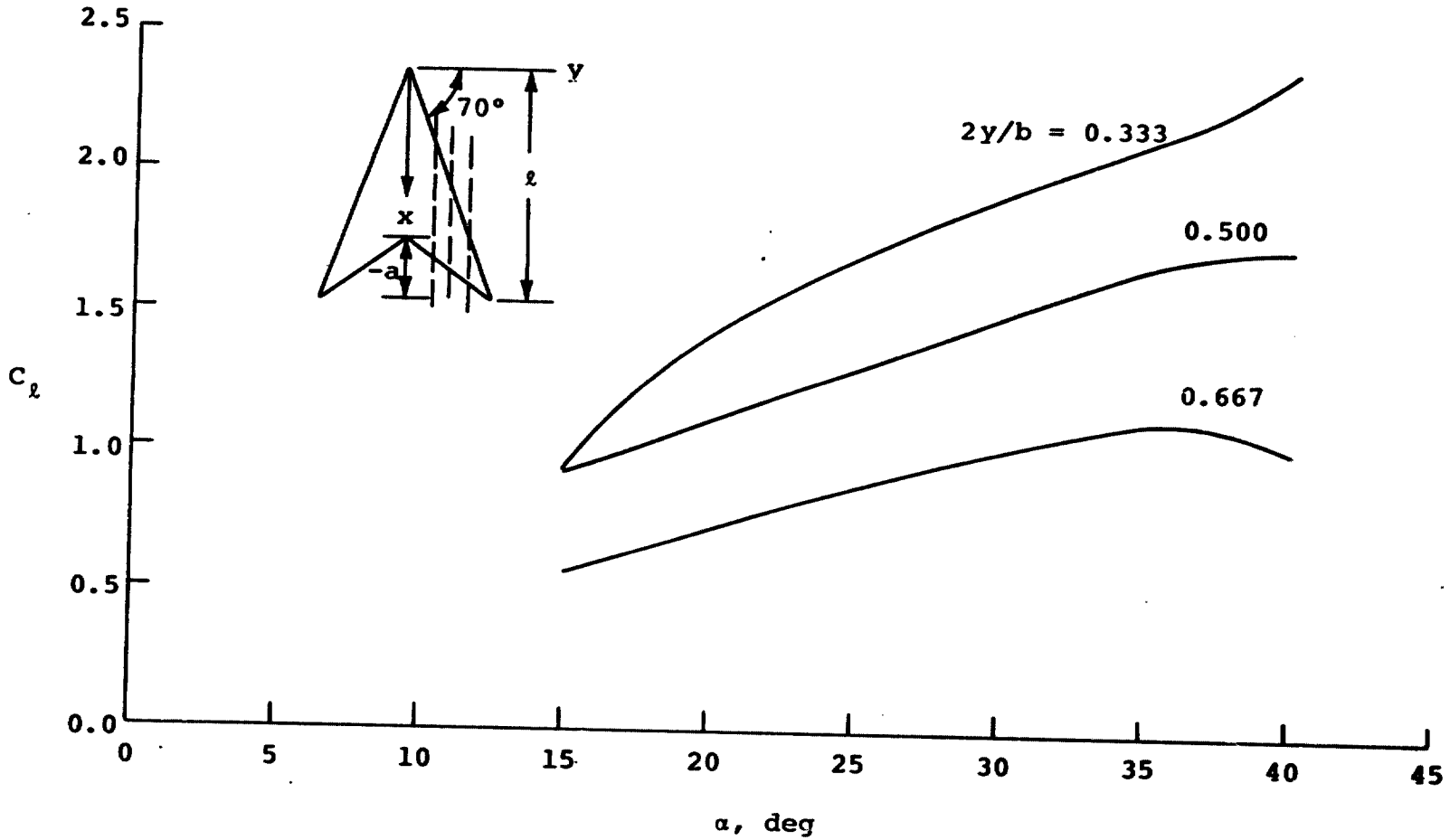

Figure 24. Variation of sectional lift coefficient with angle of attack for A = 2 arrow wing; $a/\ell = -0.273$; M = 0.

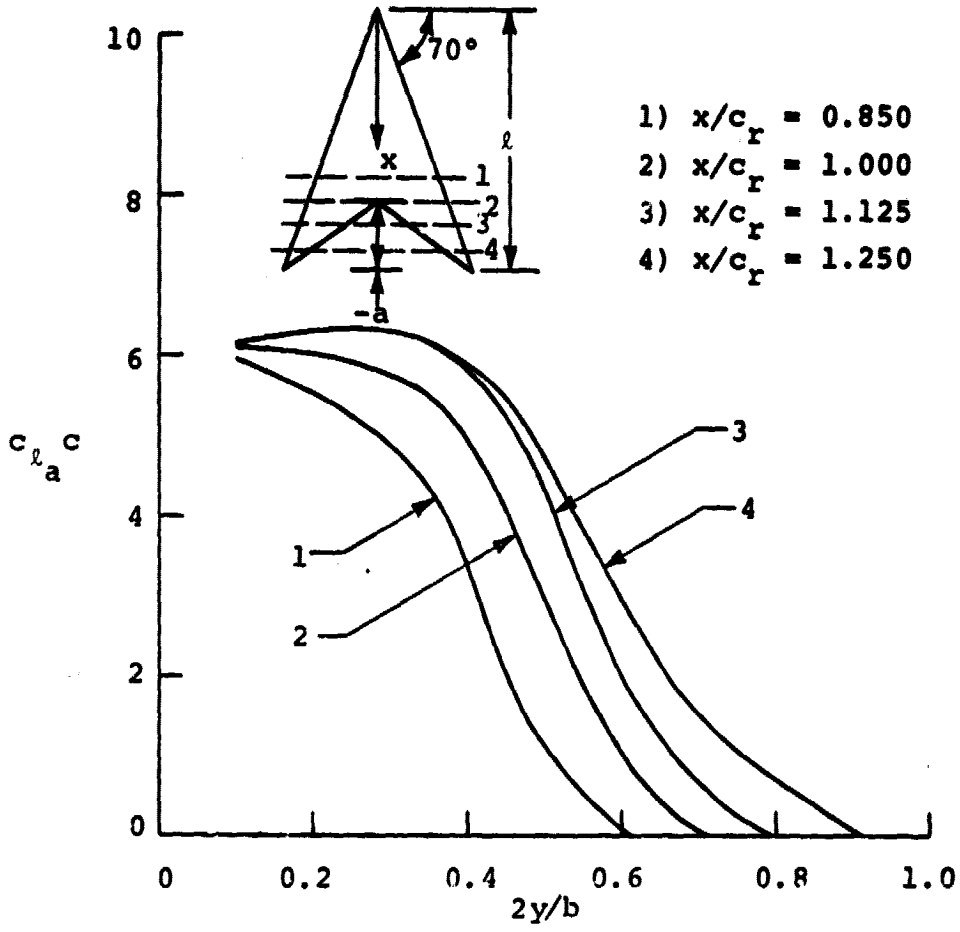

Figure 25. Accumulated span loadings for A = 2 arrow wing at $\alpha = 15°$; $a/\ell = -0.273$, M = 0.

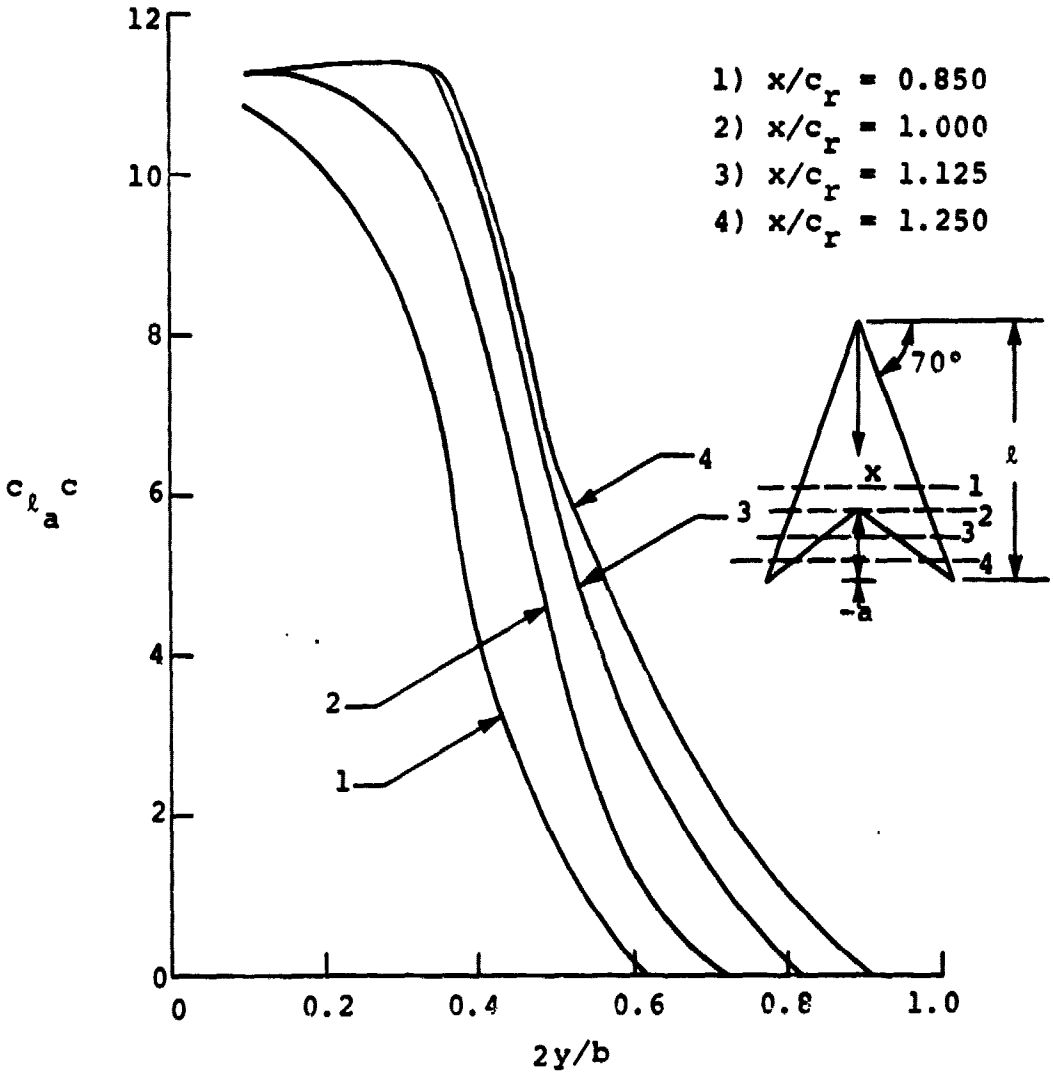

Figure 26. Accumulated span loadings for A = 2 arrow wing at α = 25°; a/ℓ = -0.273; M = 0.

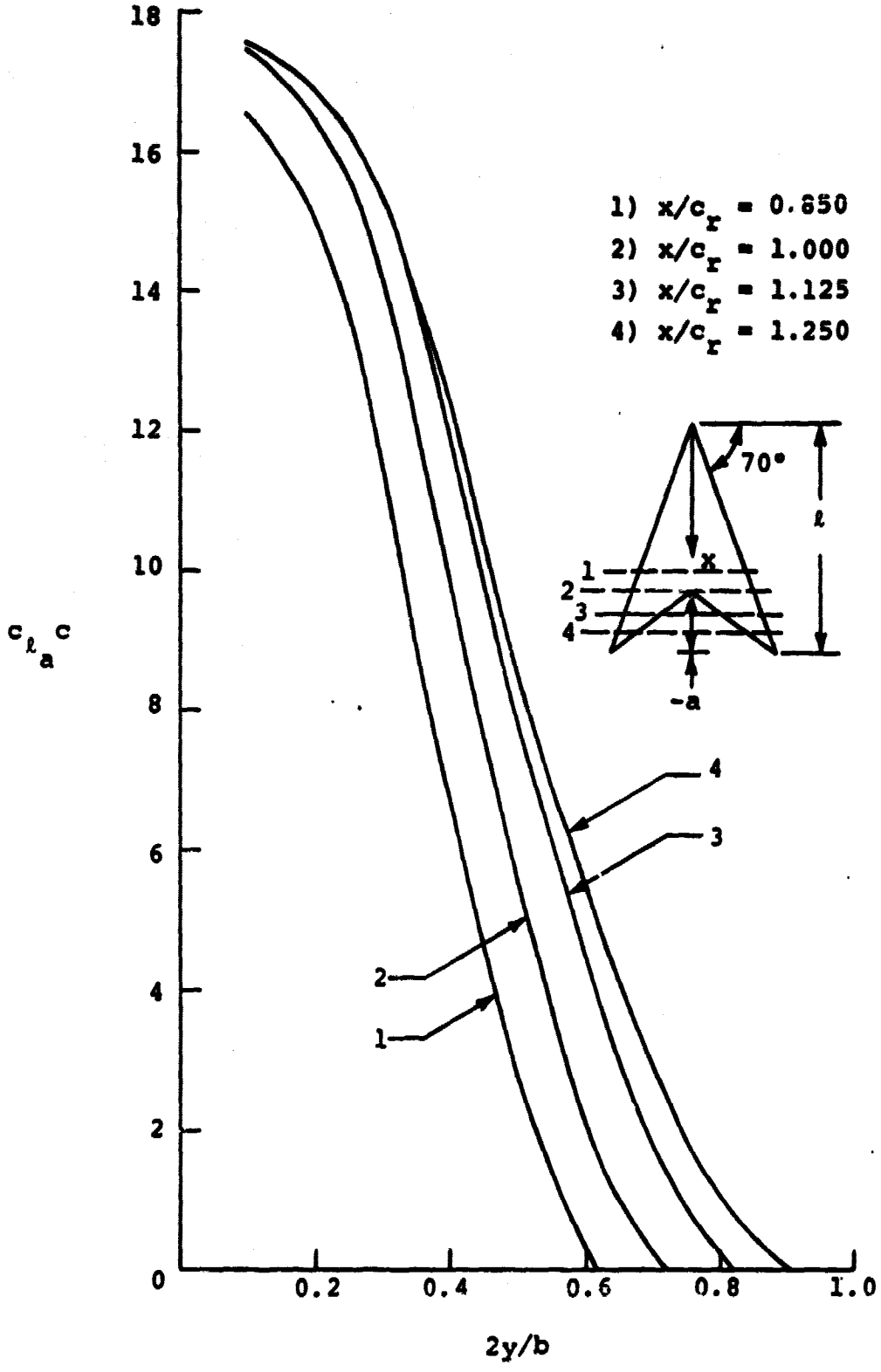

Figure 27. Accumulated span loadings for A = 2 arrow wing at α = 35°; a/ℓ = -0.273; M = 0.

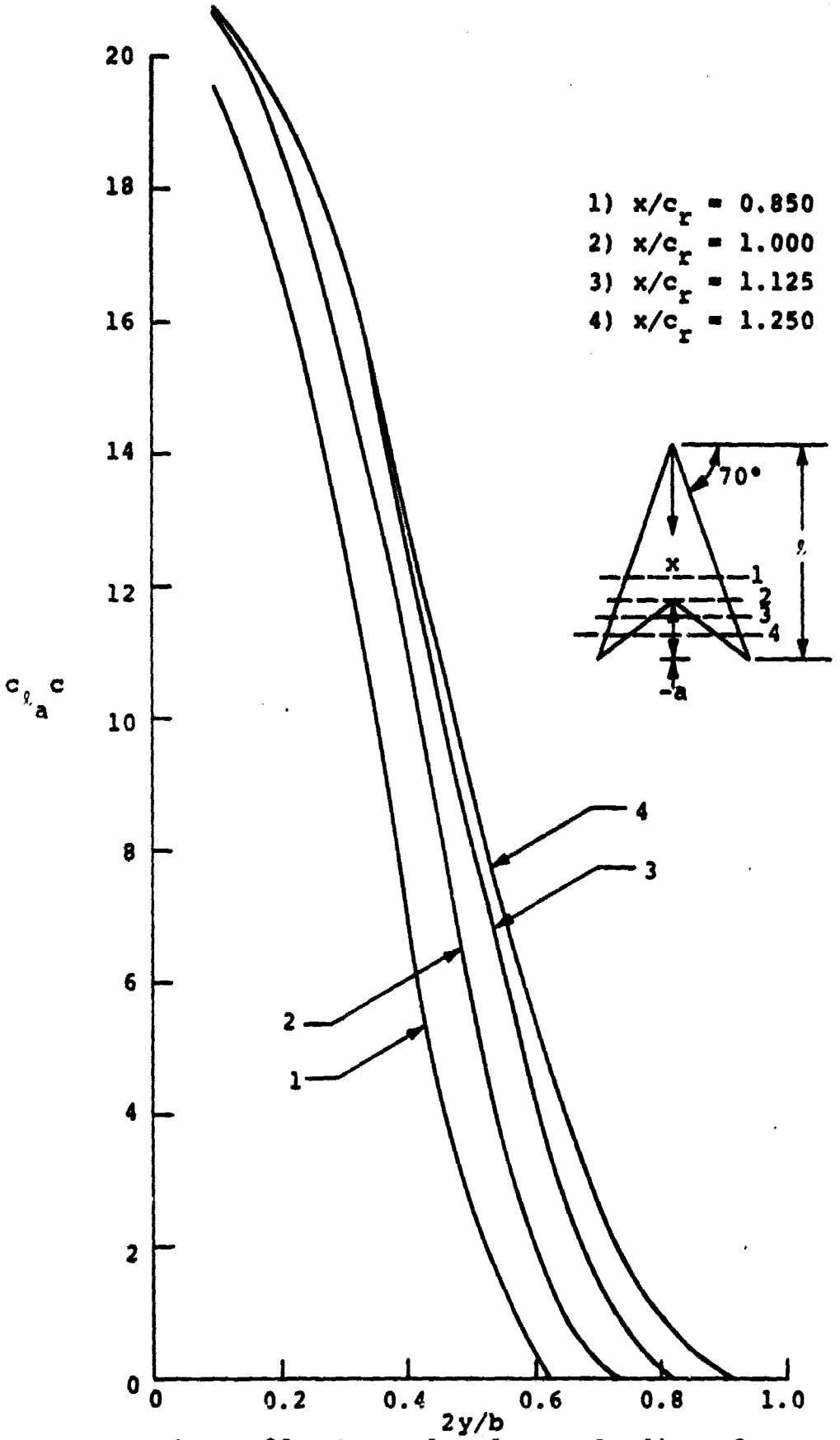

Figure 28. Accumulated span loadings for A = 2 arrow wing at α = 40°; a/ℓ = -0.273; M = 0.

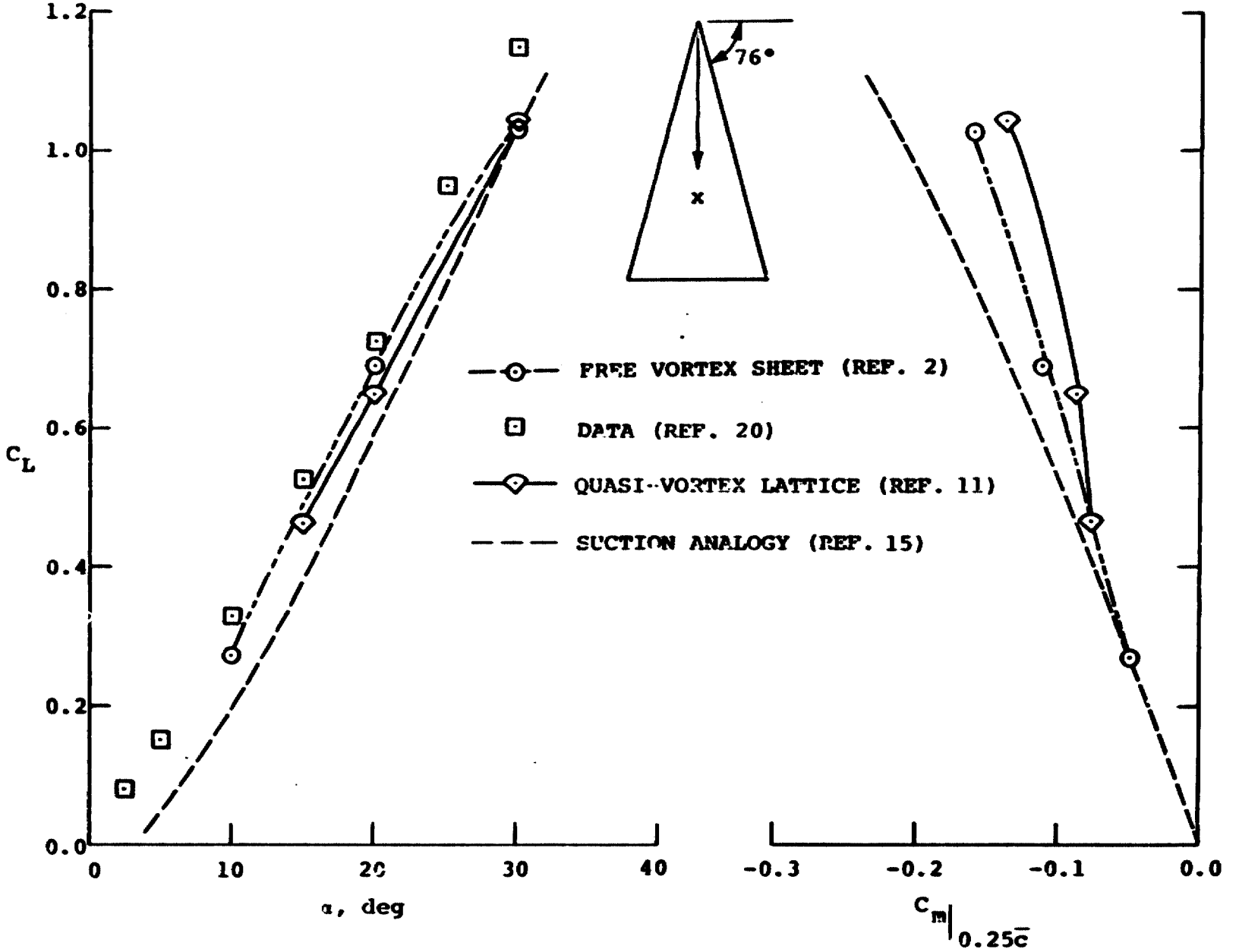

Figure 29. Longitudinal aerodynamic characteristics of A = 1 Nangia's spanwise cambered delta wing-E (ref. 20); M ≈ 0.

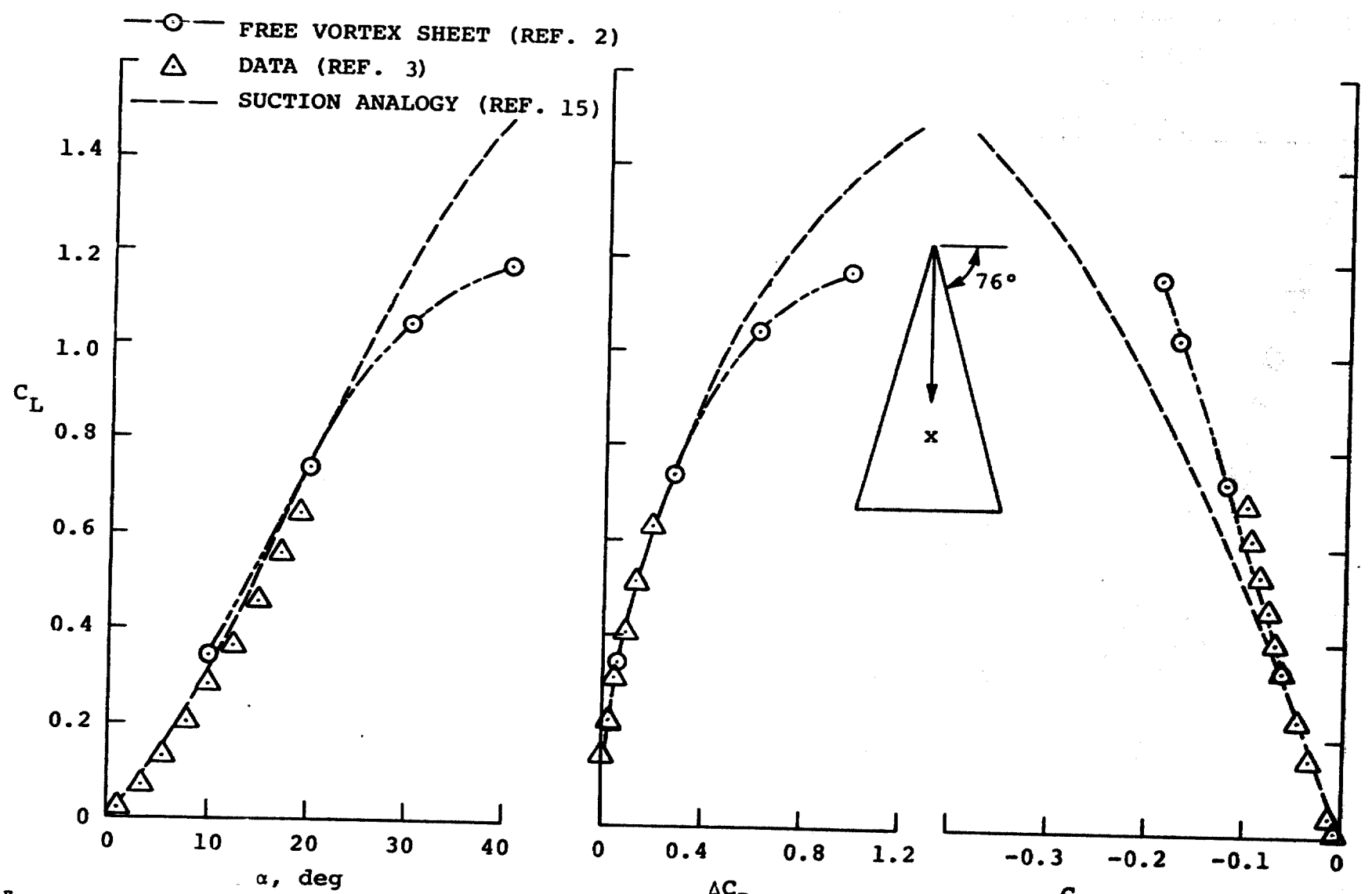

Figure 30. Longitudinal aerodynamic characteristics of A = 1 Squire's spanwise cambered delta wing-1 (ref. 3); $M \approx 0$.

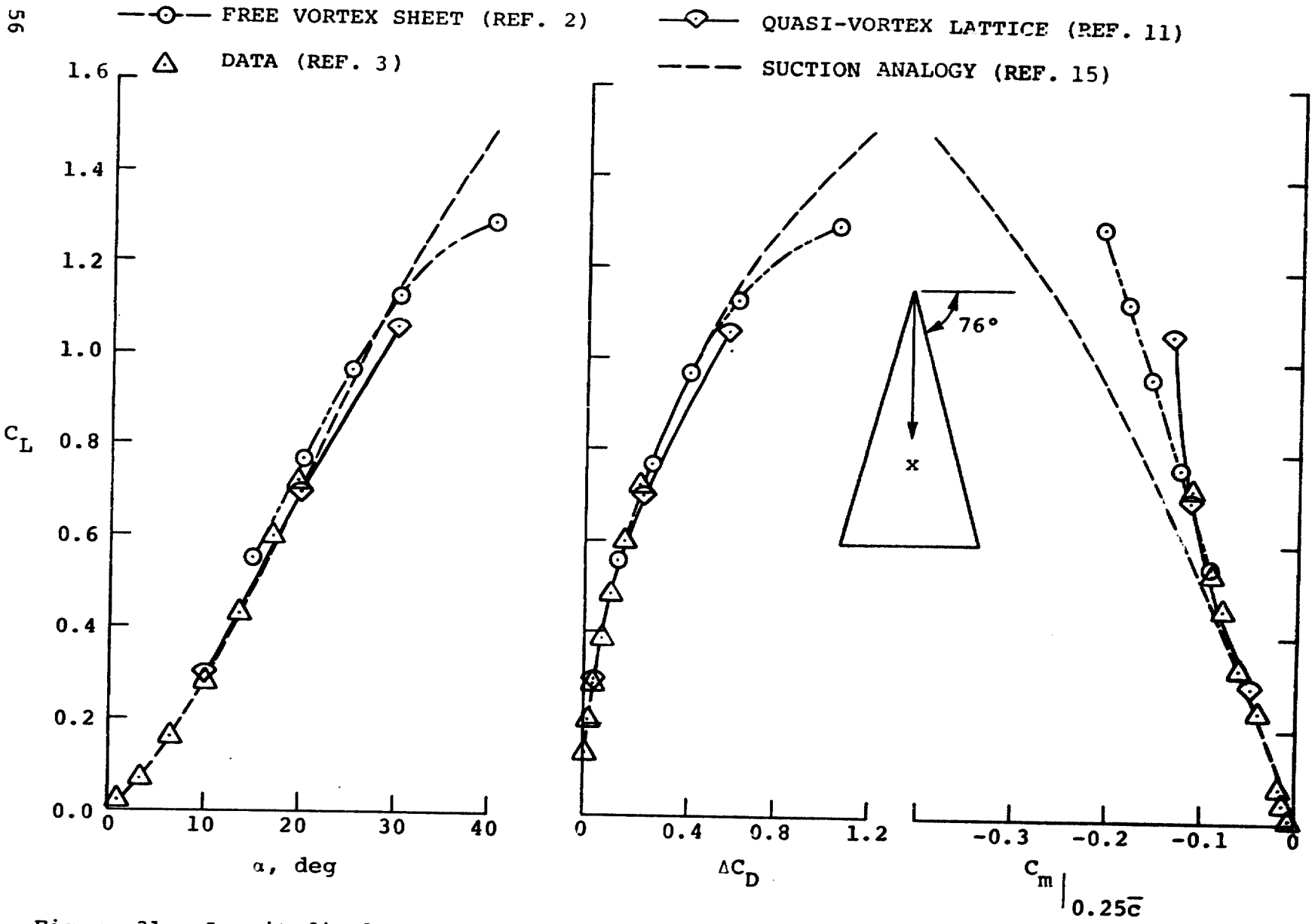

Figure 31. Longitudinal aerodynamic characteristics of A = 1 Squire's spanwise cambered delta wing-2 (ref. 3); $M \approx 0$.

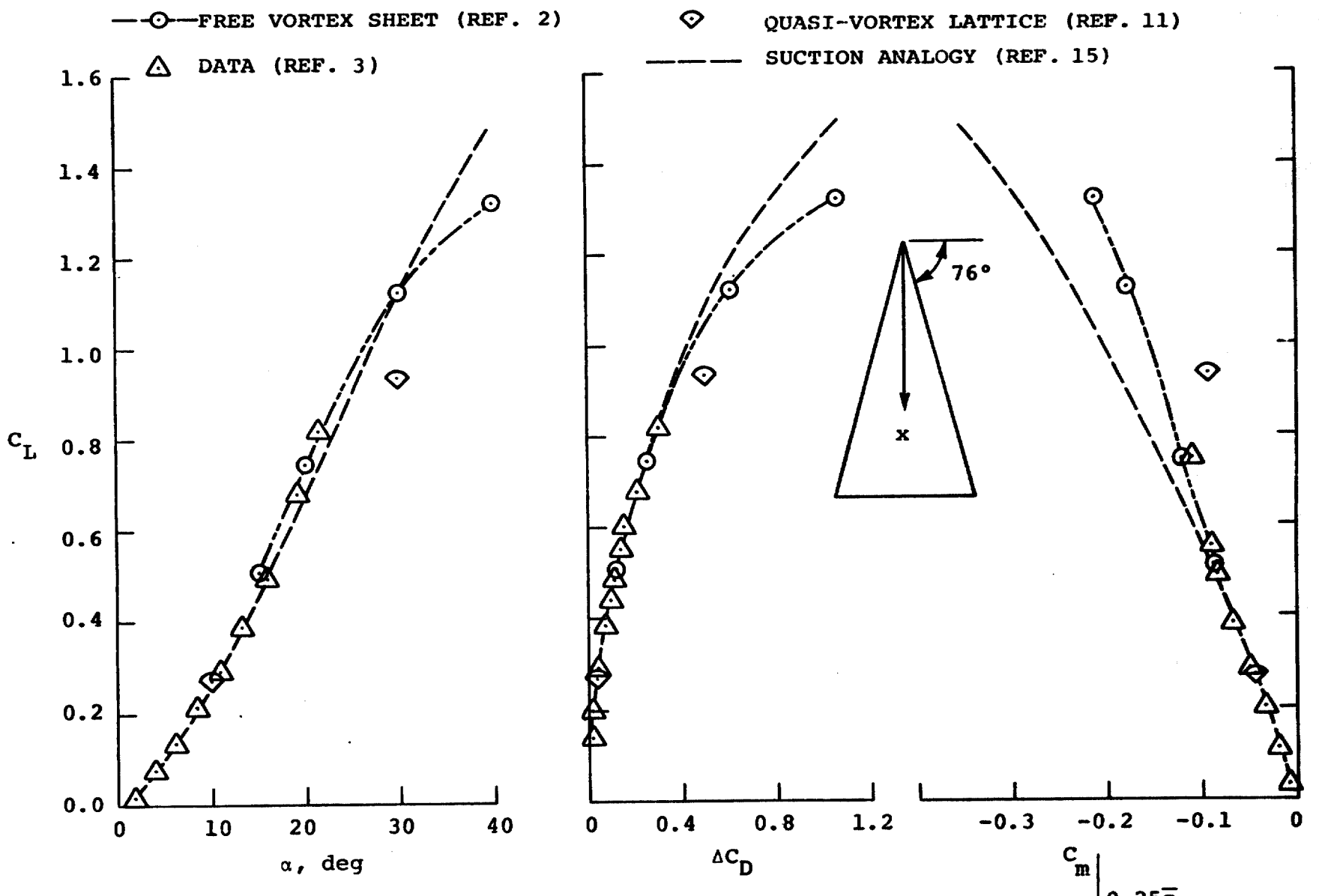

Figure 32. Longitudinal aerodynamic characteristics of A = 1 Squire's spanwise cambered delta wing-3 (ref. 3); M ≈ 0.

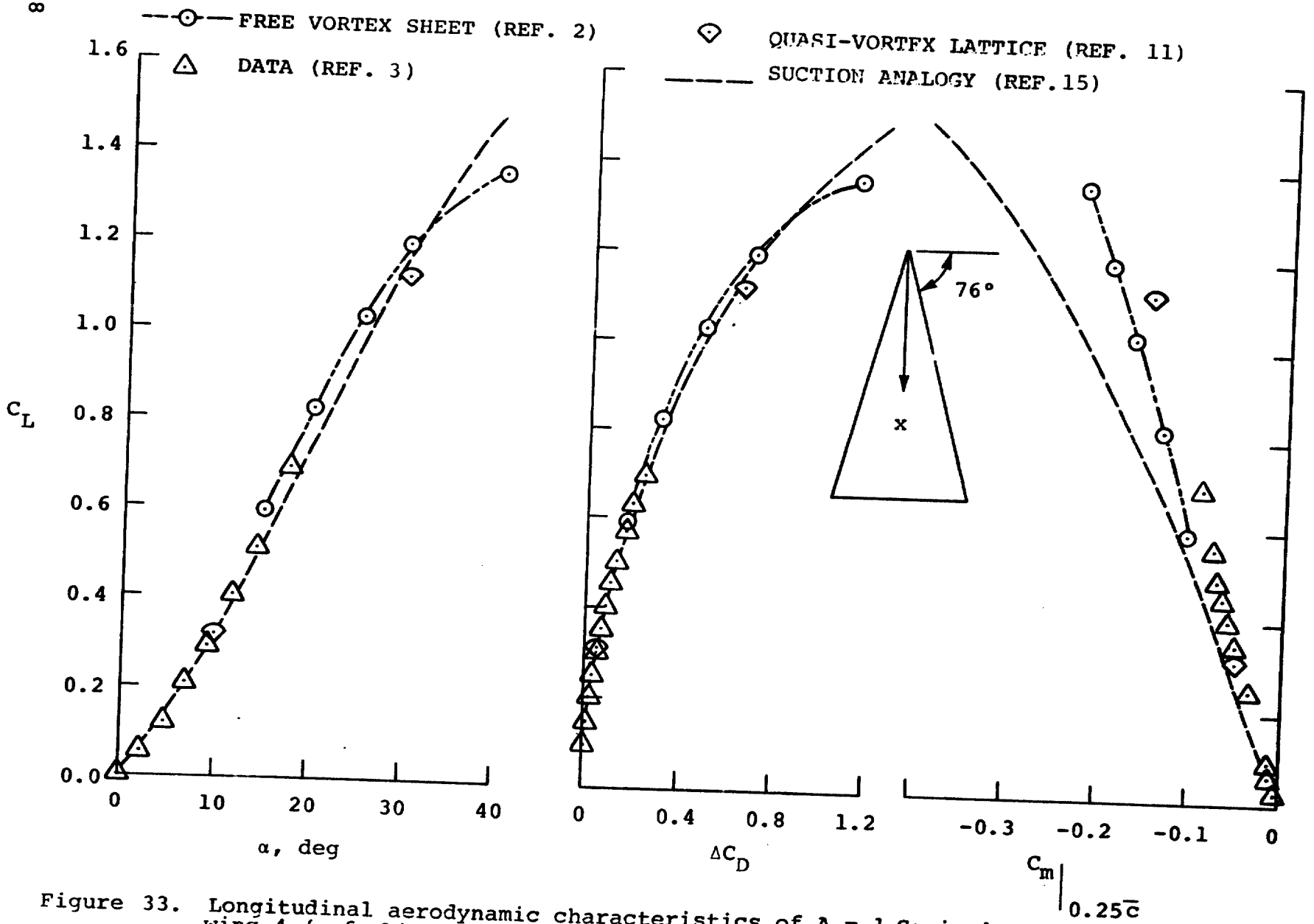

Figure 33. Longitudinal aerodynamic characteristics of A = 1 Squire's spanwise cambered delta wing-4 (ref. 3); M ≈ 0.

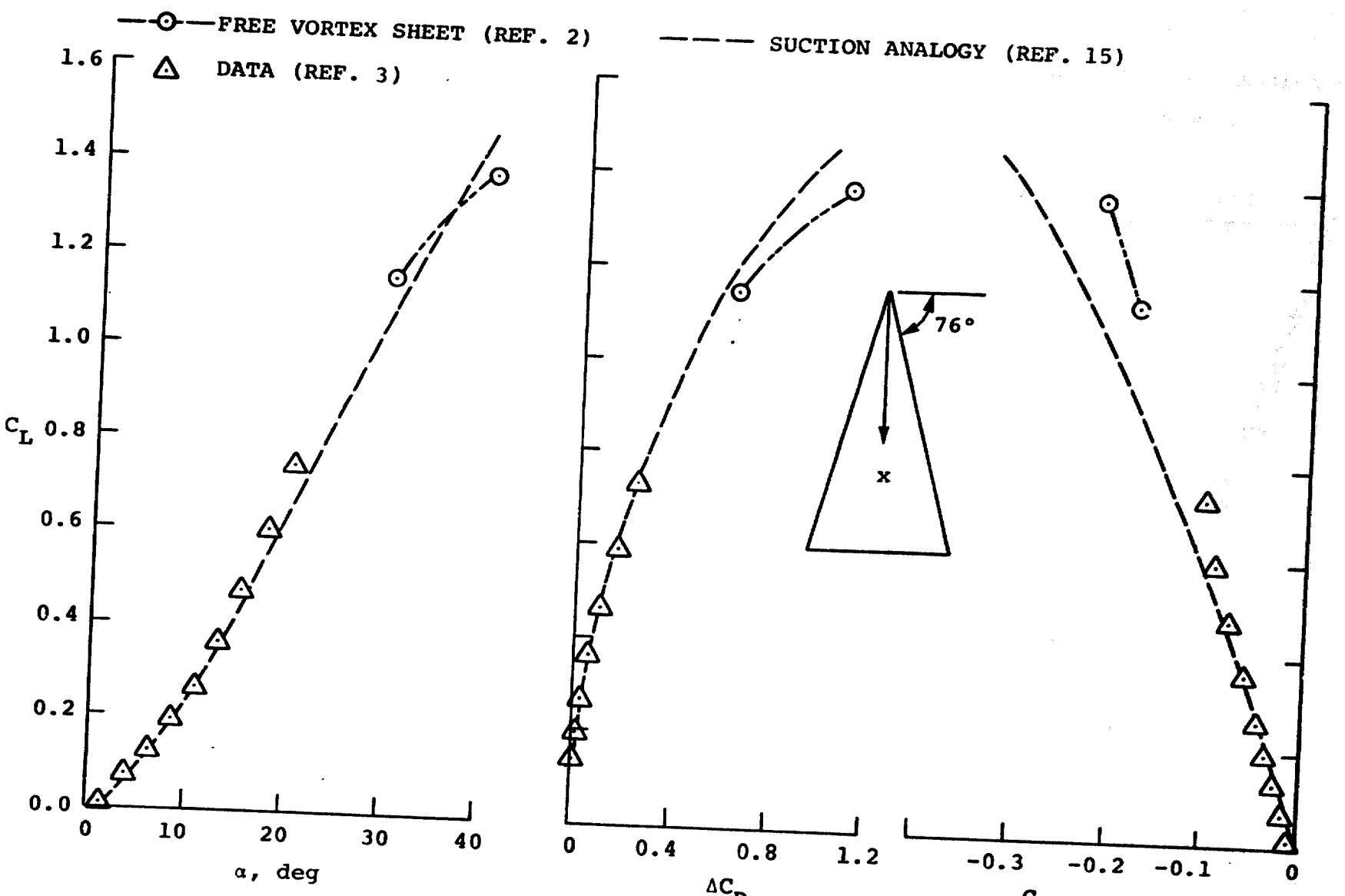

Figure 34. Longitudinal aerodynamic characteristics of A = 1 Squire's spanwise cambered delta wing-5 (ref. 3); $M \approx 0$.

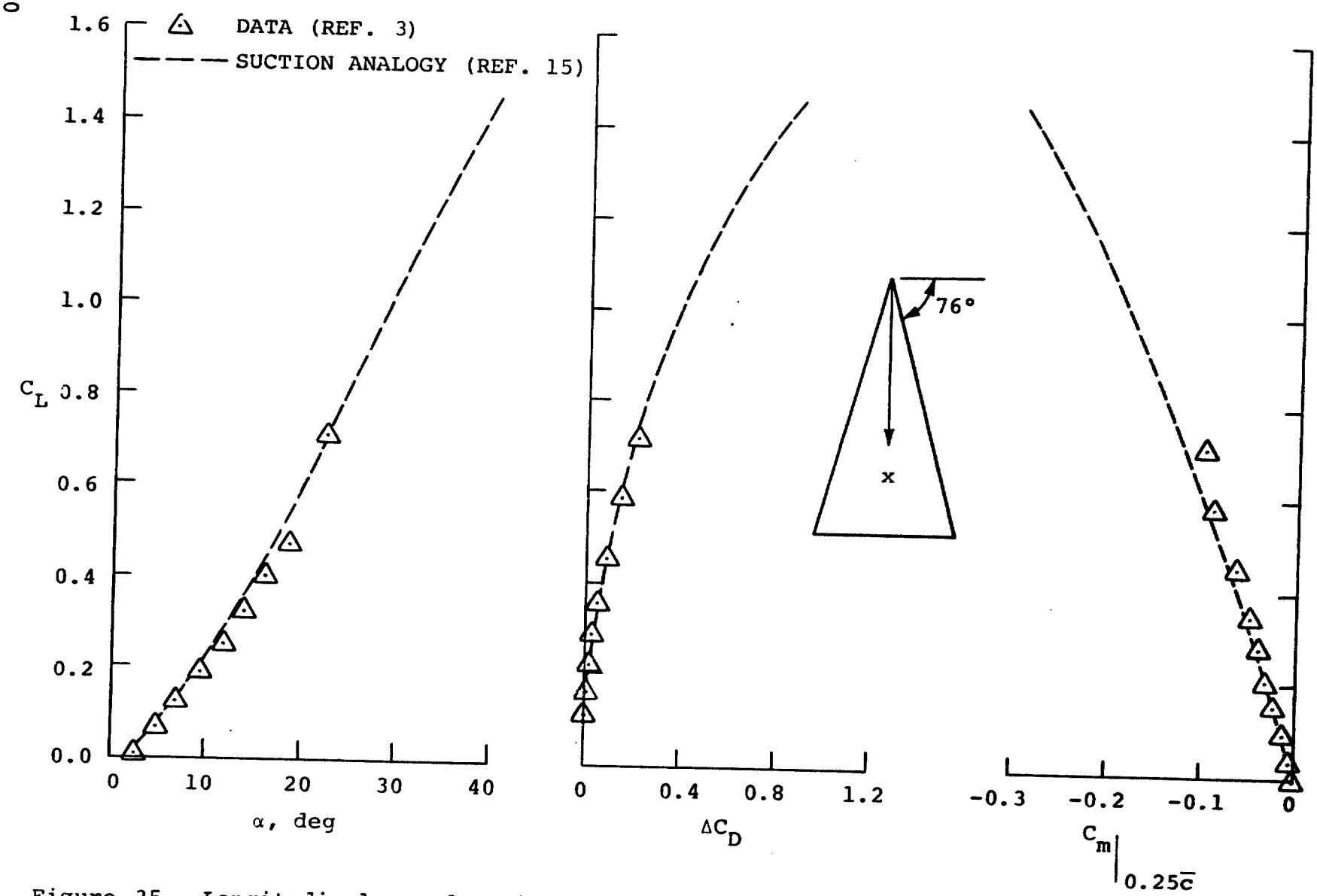

Figure 35. Longitudinal aerodynamic characteristics of A = 1 Squire's spanwise cambered delta wing-6 (ref. 3); $M \approx 0$.